Development of Photochemical Surface Modification Technique

Ellane J. Park

Submitted in partial fulfillment of the
Requirements for the degree
of Doctor of Philosophy
in the Graduate School of Arts and Sciences

COLUMBIA UNIVERSITY

2011

ABSTRACT

Development of Photochemical Surface Modification Tehcnique

Ellane J. Park

This thesis will investigate two main areas of surface modification research:

I. Designing a photoactive monolayer with improved photo-grafting efficiency
II. Fabrication of NP-Films via phthalimide self-assembled monolayer on glass surfaces

Concluding the thesis, I will briefly describe an outreach research project in collaboration with my GK-12 fellowship team.

In Chapter One, we will introduce nanotechnology and surface chemistry, with an emphasis on the use of monolayers for photochemical surface modification. The goal of this chapter is also to equip the reader with a comprehensive overview of common surface analytical techniques and a "how-to" analysis guide for thin films. Chapter Two delves into the fundamentals of SAMs and thin films – the behavior and orientation of adsorbates on surfaces, particularly at air-monolayer interfaces. We discuss the importance of studying the orientation of phthalimide-undecyl-thiol molecules on gold surfaces because the photo-reactivity (i.e. accessibility) of phthalimide terminal groups is dependent on its tilt angle, surface exposure, and packing density. One of the interesting observations includes the possibility that low packing density can potentially have higher photo-grafting efficiency.

In Chapter Three, we address the challenge of applying nanoparticles to surfaces. We introduce a fairly well known photochemical surface modification technique to

fabricate nanoparticle-films. By using a phthalimide self-assembled monolayer on a glass substrate, we photo-grafted organic nanoparticles to the surface and subsequently, produced a patterned NP-film. Using a photomask allows us to have spatial control and selection on NP-grafting.

Lastly, Chapter Four is a brief introduction and overview of the outreach project, studying the heavy metal intake of oysters in the New York Harbor. As a GK-12 fellow, I was given the opportunity to start a research project for the high school students and contribute to the New York Harbor Oyster restoration efforts. The research is focused on detecting heavy metal concentrations in oyster tissue and shells.

Table of Contents

List of Figures

Chapter 1

List of Tables

Acknowledgements

I would like to express my gratitude to my graduate advisors, Professor Nicholas J. Turro and Jeffrey T. Koberstein, whose expertise and guidance contributed greatly to my graduate research experience over the past five years. Thank you both for being supportive and encouraging through your insightful, constructive criticism.

I am grateful for all of the people who have helped me along the way, especially to the older graduate students at my introductory year to graduate research. Thank you to Dr. Gregory Carroll, Dr. Marissa Solomon, and Dr. Brian White for guiding me through the beginning and end years of my research.

Thank you to all of my collaborators – Dr. John Rabolt and Dr. Bruce Chase (Univ of Delaware, PAIR Technologies LLC) and Graduate student Siyan Zhang, Prof. Robert Prud'homme and Prof. James Link (Princeton University)

I would like to sincerely thank the members of my committee: Prof. George Flynn, Prof. Louis Brus, and Dr. Michael Steigerwald. Thank you for the enjoyable discussions.

I would like to thank my fellow teacher Sarah Gribbin, Roy Arezzo, Peter Malinowski, Nathan Dudley, Dr. Bob Newton, Dr. Nancy Degnan, Dr. Minosca Alcantara, and GK-12 LEEFS Fellowship team who have given me the amazing opportunity to teach at the Harbor School. I looked forward to my weekly commutes to governor's island to teach chemistry labs and enjoyed working on the oyster restoration project.

Thank you to all the members of the Turro and Koberstein groups. You have helped me over the years with interesting discussions and constructive critique on my practice presentations.

Thank you to my friends from Redeemer Presbyterian Church who have always been so supportive in prayer and encouraging words. I am also grateful for the support from my friends in the Chemistry Dept and some who have shared a common interest in Women in Science at Columbia – Julia, Judy, Michelle, Teresa, Sharon, Qing, and Rachel.

Lastly, to my family, thank you for being supportive through my many years of school. You have always inspired and pushed me to make big accomplishments. Thank you!

To my family and friends

1 Introduction to Photochemical Surface Modification

Surface chemistry, the study of chemical reactions at interfaces, has a significant presence in nature as exemplified in Figure 1-1. On the macro-scale, a large body of water meets air at the air-water interface while there is an expansive surface area of solid-air interfaces across a forest of trees. On the micro- and nano-scale, as you examine a leaf closely, photosynthesis takes place at the water-membrane interface of chloroplast cells. Interfacial chemistry is a critical component of essential chemical processes such as photosynthesis. This area of study is oftentimes at the forefront of developments in biomedical and technological applications due to its unique ability to change surface properties without altering the bulk material. For example, a biomedical device may not operate desirably because the surface is interacting too strongly with cells and proteins in physiological conditions. A common solution involves coating the surface of the device with an anti-biofouling layer to deliver its optimal performance without changing the core technology. Changes at the surface level can also be seen to be economically efficient, as the bulk material itself does not need to be compromised.

Due to the powerful ability that surface chemistry has in shaping the macroscopic world, surface engineering techniques are being used in a wide range of industries including electronics[1] and biomedical[2]. Because the ability to control the chemical and physical properties at surfaces is very important, general surface engineering methods need to be developed. This thesis will introduce surface modification techniques based on photochemical reactions and cover analytical methods that are used to study these interfacial changes on a nanoscopic level.

Figure 1-1. Interfaces can provide functional properties at the air-water, water-solid, and solid-air interfaces on the macro- (left) to micro/nano-scale (top right; bottom right).

1.1 History and Fundamental Study of Monolayers

Self-assembled monolayers (SAMs) have been extensively studied for the ability to control surface properties that has important implications from the point of view of both fundamental and technological advances. In 1983, Nuzzo and Allara[3] discovered the chemisorption capabilities of dithiols to form ordered SAMs on gold surfaces. Since then, further studies have demonstrated the differences in structure between long- and short-chain thiol monolayers by using surface techniques such as optical ellipsometry, infrared spectroscopy, and electrochemistry.[4] Porter et. al. proved that SAMs of long-chain thiols on gold have strong potential as model systems for studies of heterogeneous electron transfer, ion transport, and double-layer phenomena. These results further reveal the significant role that organic molecular structure plays in the overall structure of monolayers. Consequently, the preparation and structural characterization of SAMs are of great interest in a variety of interface applications from catalysis[5] to biomedical

applications[2, 6]. Two methods were predominantly used in SAM preparation: Langmuir-Blodgett techniques,[7] involving the transfer of an assembled film at an air-water interface to a solid substrate, and self-assembly,[8] based on the natural occurrence of molecules in solution adsorbing onto a substrate. A substrate is referred to as material that provides the surface on which something is deposited, in this case, the deposition of SAMs. For example, the silicon wafer used to manufacture integrated circuits. Commonly studied SAM systems include chlorosilanes on silicon,[9] carboxylic acids on metal oxides,[10] and organosulfur compounds on gold[3, 11]. SAMs of organosulfur compounds on gold will be the system of focus in the introduction because they are, in general, the most studied and understood.

Optimal preparation methods have been developed to produce highly ordered, supported monolayers with wide range of choices for the functional group (terminal group) located at the ambient interface. Surface functionalization of hard substrates generally requires the synthesis of organic molecules with three constituents, each with an important function in the self-assembly process. As illustrated in Figure 1-2, each organic molecule consists of a sticky foot (SF), molecular spacer (SP), and terminal group, in this case, a photoactive group (PA) and collectively, the organic molecules spontaneously assemble onto a substrate as an ordered monolayer.

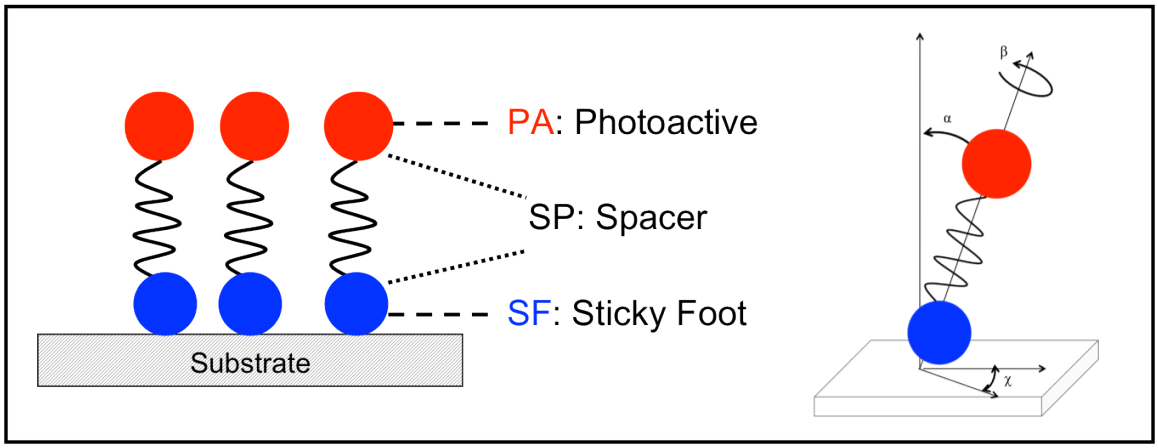

Figure 1-2. Schematic illustration of an idealized self-assembled monolayer with a photoactive group (PA) exposed at the air-monolayer interface.[12]

1.1.1 Self-Assembly Process

The organized structure is formed by a directed self-assembly process as shown in Figure 1-3. Initially the molecules orient themselves close to the air-water interface before the substrate is immersed into solution (not shown). When the substrate is immersed into solution, the molecules are observed to physisorb to the surface until the sticky foot (SF) group provides anchoring to the substrate via a covalent bond. The SF group determines the lateral positioning of the molecule on matrix surface, and until recently, believed to orient the molecule such that the photoactive moiety is presented at the monolayer interface (Figure 1-3A). However, recent studies[13] have surfaced the argument that the SAM molecules initially orient themselves in a "lying down" phase before orienting its PA group to the solvent-monolayer interface, as illustrated in this figure.

From the lying down phase, the spacer groups contribute to greater order of the monolayer as the attractive in-plane van der Waals interactions play a significant role in driving molecular assembly (Figure 1-3 B). When the SF-substrate interactions are stronger than the intermolecular interactions, the molecules form a film on the surface via

covalent bonding with or chemisorption onto the substrate. For example, thiol, disulfide and alkyne groups are known to have a strong affinity for gold substrates.[14] The intermolecular interactions may be due to strong van der Waals interactions that are attributed to hydrocarbon chains, which are typical of SP groups. The degree of intermolecular interactions depends on the alkyl chain length – as the number of carbons in the chain increase, the van der Waals interactions grow stronger.

With the interplay and balance between the SF-substrate and van der Waals interactions, the idealized SAM is densely packed and highly ordered as illustrated in Figure 1-3C. However, the impossibility of eliminating all SAM defects is well understood. In the next section, we will discuss the factors that affect the quality of SAMs.

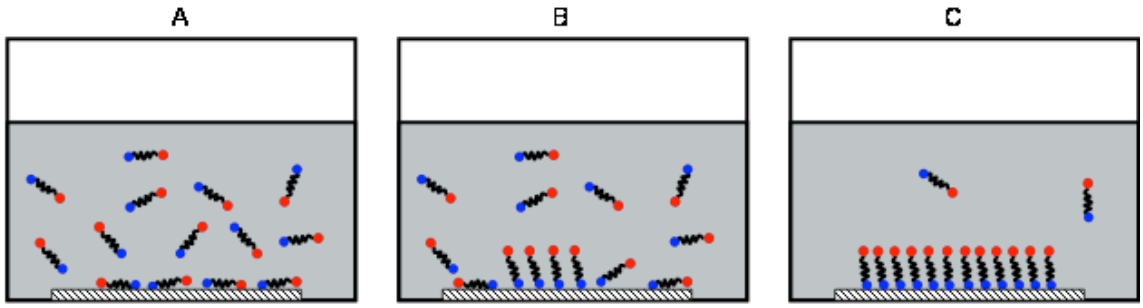

Figure 1-3. Schematic Illustration of Self-assembly process.

1.1.2 Quality of SAMs: Defects, Density, Order

While the resulting SAM in Figure 1-3 is sketched as a perfect monolayer with the molecules in a closely packed conformation, this image is far from real. In fact, there are several types of defects[13a] that can influence the performance efficiency of SAM-coated devices, in the case of sensors, for example. There are some strategies used to minimize the effects of these defective monolayers, but it is important to realize that they

will always be present. We will explore these possible defects at the molecular level, as illustrated in Figure 1-4.

In general, the monolayers tend to deviate from well-arranged structures such as Figure 1-4 and exhibit structural defects and disorder when there is a mismatch between the various types of interactions. Detailing the possible molecular arrangements gives us a better understanding of the factors that may cause structural defects in monolayers.

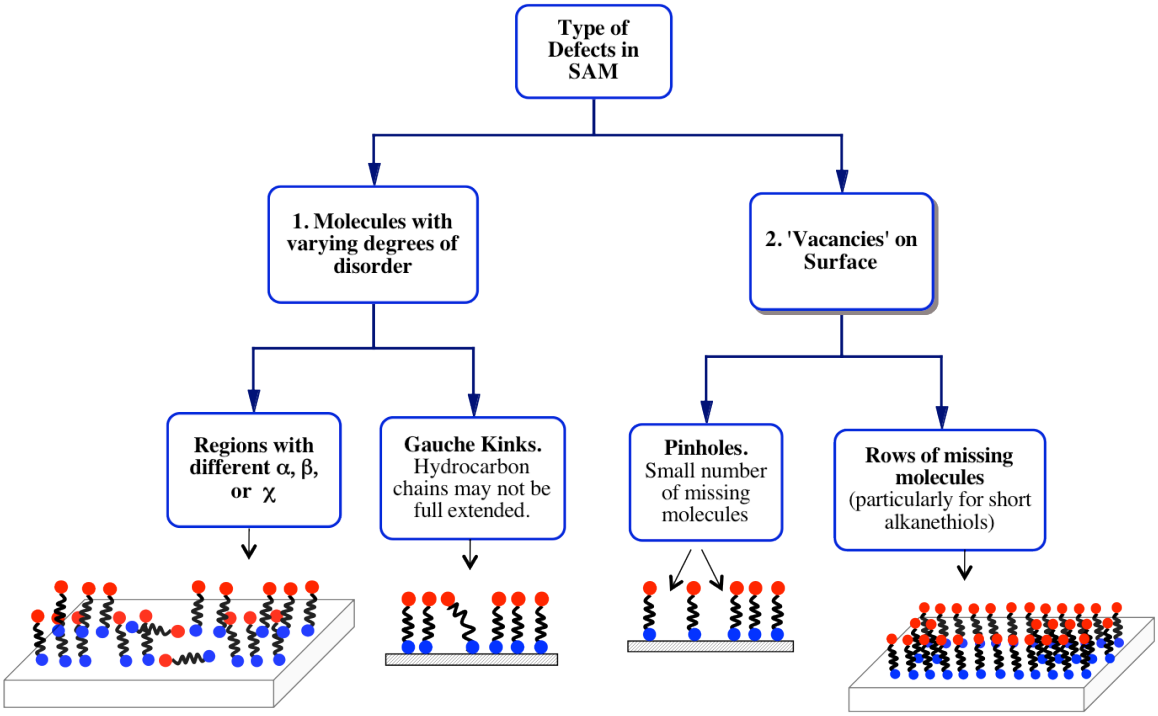

Figure 1-4. Overview of possible defects in SAMs[13a]

Knowing these fundamental chemical and physical interactions is key to controlling the formation, structure, and reactivity of chemically modified surfaces. The approach to studying these SAMs has *two integral parts*: the proper selection of molecular systems that allow us to probe these interactions that direct the attachment, orientation and packing density of the adsorbates, and the search for useful characterization tools to apply to these systems. Moreover, theories and experimental

results that detail the self-assembly process itself determine the orientation of molecules on surface and overall structural information of monolayers.[13b, 15] We are interested in understanding how the orientation of the adsorbate's photoactive terminal group will affect its photo-reactivity (grafting external species) at the air-monolayer interface.

Factors that affect the density and ordering of SAMs include temperature, nature of terminal groups, adsorption time, hydrocarbon chain length, and substrate quality. With increase in temperature, there is an increased occurrence of gauche defects. The chemical nature of the photoactive groups are very important. As varying groups (-SH, COOH, OH and NH_2) are introduced as opposed to a terminal methyl group, there is typically a *decrease* in SAM ordering. The effect of the terminal group on the chain ordering (hydrogen bonding, electrostatic interactions) is still not completely clear. In particular, the effect of solvent, pH and surface topography should be carefully investigated in this matter. Other factors, as mentioned, are adsorption time, hydrocarbon chain length, and substrate quality that make significant changes in how a monolayer is assembled naturally.

1.2 Design and Engineering of Nanoparticle-Films: Photo-grafting

1.2.1 Introduction

SAMs alone have pioneered the history of surface modification, but in the area of device fabrication, SAMs are used as building blocks in sensors, biosensors, actuators, and molecular motors.[16] SAMs can be used to graft a new species such as biomolecules, polymers, or nanoparticles to a surface. Surface modification methods can range from organic synthesis[17] to photo-chemistry[6], particularly focused on grafting polymers and biomolecules. This thesis will explore the design of photoactive SAMs and its role in the

engineering of nanoparticle-films (NP-films). As illustrated in Figure 1-5, SAMs can be used to covalently bind any external species (represented by white squares) upon light exposure. NP-films are typically prepared by lithography, a costly technique that requires a complex infrastructure setup and produces unstable films due to non-covalent NP-attachment to the surface. With limited techniques available, it is desirable to develop a simple approach that fabricates covalently bound NP-films.

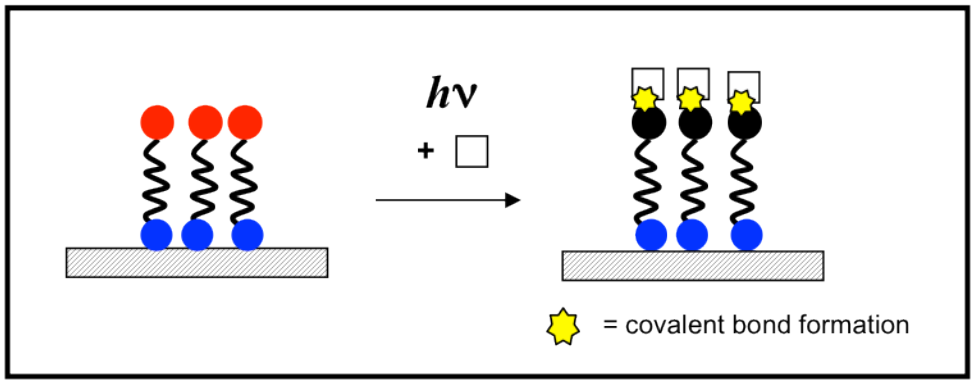

Figure 1-5. Schematic illustration of photo-grafting ability of SAMs. White squares represent external species (e.g. biomolecules, polymers, nanoparticles) that are photo-grafted to the surface.

Here, we propose to deposit the NPs onto a monolayer-functionalized surface by spin-coating and then exposed to UV light to form covalent bonds at the NP-monolayer interface. Spin-coating[18] a solution of the nanoparticles (Figure 1-6; left) allows for a dry deposition of NPs (Figure 1-6; right) by spinning the surface at a high speed and evaporating the solvent. Spin-coating is a convenient way to produce a physisorbed layer of the NPs, but there are some issues such as NP aggregation that will be addressed in Chapter 3. Upon spin-coating, the NP-films are exposed to UV light to activate the photoactive SAM. This method is commonly referred to as photo-grafting and patterning when using a photomask.

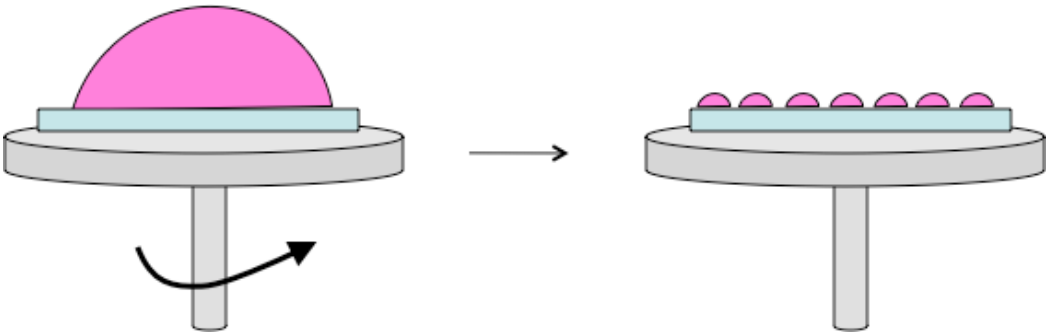

Figure 1-6. Schematic illustration of spin-coating a solution of nanoparticles.

1.2.2 Photo-Grafting and Patterning Surfaces

Both SAMs and NP-films provide interfaces that can be modified in order to instill a surface with a new physical or chemical property. Using light to perform this surface chemistry is one of the cleanest surface modification methods. Photochemical methods also provide the opportunity to pattern a surface by using a photomask because photons have the ability to penetrate through the smallest spaces in a mask (Figure 1-7). Using light to perform chemistry at interfaces allows for control over spatial deposition of various materials such as proteins[19], DNA[20], and nanoparticles[21]. Photochemical methods can be carried out on SAMs and thin films to make chemical and physical modifications at the interfacial level.

Photoactive SAMs present preprogrammed terminal groups at the air-monolayer interface that chemically transform upon exposure to light. The nature of the PA group not only determines the surface chemical properties, but also controls surface physical properties such as wettability and adhesion.

Among the various surface photoreactions[12], the concept of photo-addition, commonly known as surface photografting, is most relevant to this thesis. Photografting

can be approached in two ways: the photoactive (PA) group can be located on the external species that is immobilized onto a derivatized substrate (referred to as "grafting-to") or the PA group can be located on the substrate itself (referred to as "grafting-from"). For the purpose of this thesis, we will focus on the photografting-from method. These photo-transformation methods are typically applied through a photomask (as shown in Figure 1-7) to achieve patterned deposition of external species, such as proteins, DNA, and nanoparticles. The feature size of the mask pattern and wavelength of incident light determine the resolution of such patterns. As a result, light penetrating into small spaces allows for high spatial selectivity compared to other lithography techniques used for surface patterning.

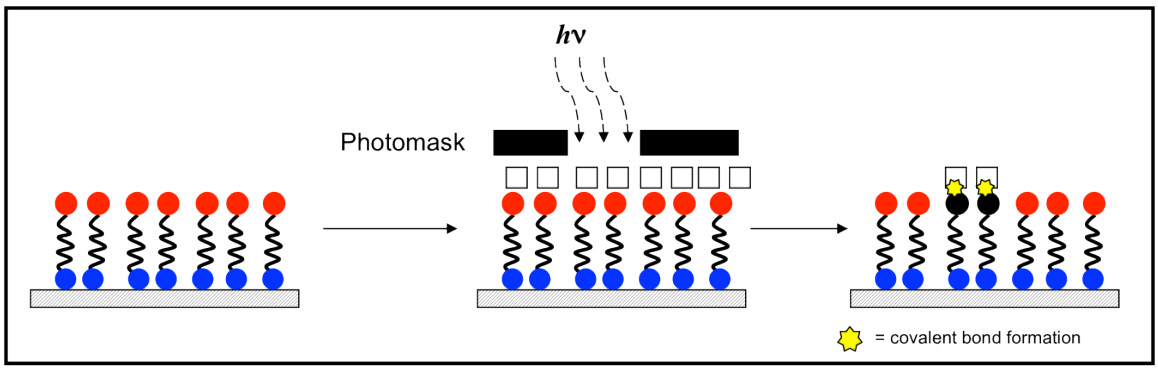

Figure 1-7. Photo-patterning scheme. All of the photo-induced surface modification reactions can be patterned onto self-assembled monolayers on hard and soft substrates by using a photomask.

1.2.3 Selection of Photoactive Molecule

Commonly used photografting methods originate from a well-known photochemical mechanism called hydrogen abstraction (Figure 1-8). Hydrogen abstraction occurs when there are two types of species present: carbonyl group that is excited and an external species that has a hydrogen readily available. The photo-grafting approach relies on the selection of photoactive functional groups that react directly with

C-H groups have been incorporated into a variety of surfaces. The photoactive groups utilized in such a mechanism include aromatic ketones, diao compounds and azides.[12]

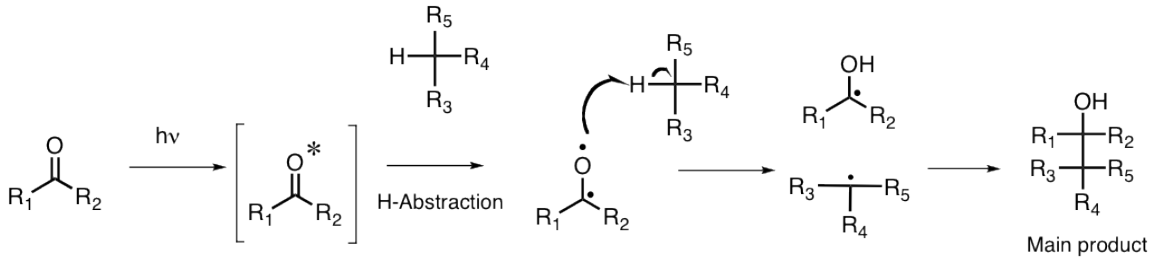

Figure 1-8. Hydrogen Abstraction Mechanism for carbonyl containing photoactive groups.

Of the various families, benzophenone (BP) derivatives are the most commonly used in the immobilization of polymers to a variety of surfaces as schematically illustrated in Figure 1-9.[22] BP delivers one of the best chemical functions under various conditions of light and solvent. BP derivatives are excited at a wavelength of approximately 350 nm[22b], which helps avoid protein-damaging wavelengths. Compared to other photoactive groups such as aryl azides, diazirines, and diazo esters, BPs are chemically more stable.

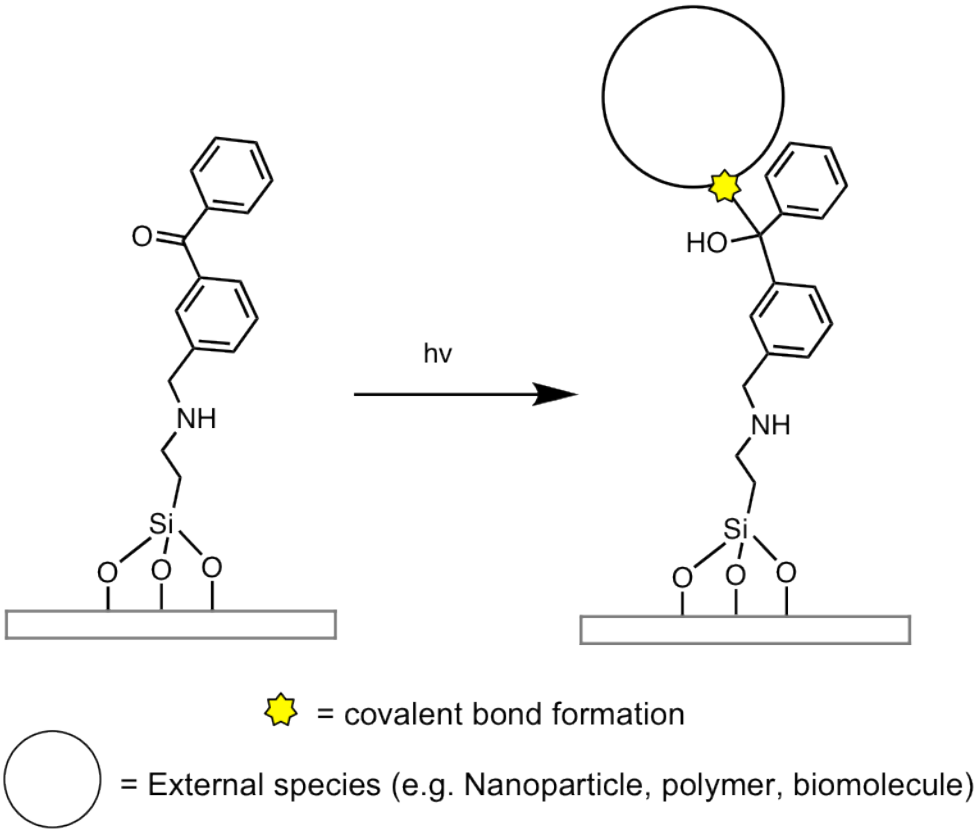

Figure 1-9. Benzophenone-functionalized surface used in photo-grafting any external species (represented by circle).[22e]

Monolayers with phthalimide chromophores[6, 23] have delivered similar results as BP-monolayers. However, phthalimide derivatives are excited at shorter wavelengths averaging at 254 nm in wavelength. Comparing the chemical properties of a phthalimide with a BP, we observe that the imide functional group makes the overall chemical structure more hydrophilic than BP. Consequently, the more hydrophilic nature of phthalimide-monolayers affects the surface wettability and therefore, the grafting efficiency of an external species. For example, carbohydrates (hydrophilic) will more easily wet a phthalimide-monolayer surface as opposed to a BP-monolayer and consequently, can produce carbohydrate-films with greater thickness and coverage.[6]

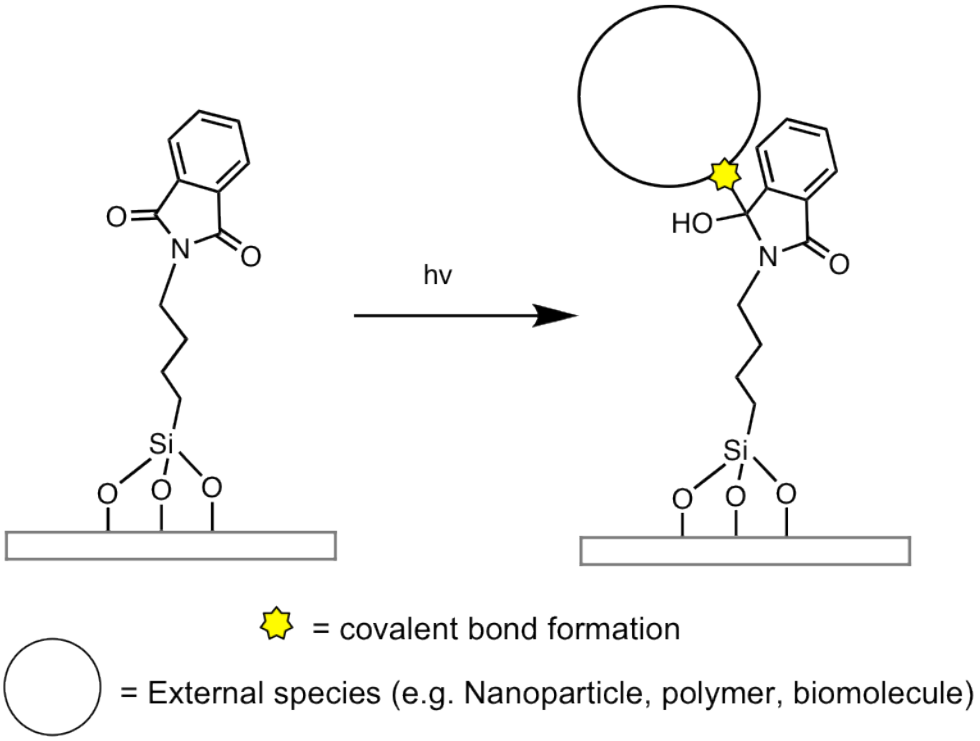

Figure 1-10. Phthalimide-functionalized monolayer undergoes a hydrogen abstraction to covalently bind an external species (represented by the circle) to surface. The hydrocarbon chain (linker) can be varied to give the monolayer different physical properties, thereby possibly altering the photoreactivity of the phthalimide chromophores.

BP and phthalimide derivatives have been utilized in the form of self-assembled monolayers to photograft biopolymers onto surfaces but no quantitative analysis has been conducted to calculate their photografting efficiency. Comparing the two PA groups, we determined phthalimide SAMs to be more advantageous, owing to better wetting capabilities and higher surface tensions.[6] As Chapter 3 will introduce, the better wetting capability of the phthalimide SAM allows for hydrophilic molecules to more strongly adhere to the surface and increase chances of greater photo-grafting efficiency.

1.2.4 Selection of Substrate

The depth and quality of analysis for monolayers and thin films can depend heavily on the selection of a substrate. For example, selecting a gold surface will open opportunities to use techniques such as Infrared Grazing Incidence Reflection (GIR) and Surface Plasmon Resonance Spectroscopy (SPR). These techniques will be reviewed in Chapter 1.3.

The photochemical surface modification method can be applied to both hard and soft substrates. The design of the project also plays a role in this selection process. If the project has biomedical applications in the development of diagnostic devices, the substrate of choice is 'hard' (e.g. glass or gold). On the other hand, if the project has aerospace engineering applications, most surface chemistry involves the use of paint, which is a 'soft' polymeric base.

Hard substrates range in a variety of choices from metal (e.g. Au, Ag, Cu) to non-metal (e.g. glass, quartz). In Chapter 2 of this thesis, the concept self-assembly on gold surfaces will be introduced. For this particular project, gold was chosen to be the ideal substrate for the following reasons. First, gold exhibits a low chemical reactivity and provides the opportunity to apply both vibrational spectroscopic and electrochemical techniques. Secondly, gold can potentially enhance the photochemistry of the PA group in the SAM due to surface plasmons and possible energy transfer. Thirdly, using gold substrate allows for a wider selection of techniques to study the molecular system. In Chapter 2, the hard substrates used were glass and silicon, which made the use of techniques such as SPR not possible.

1.3 Review of Surface Characterization Techniques

This section is to serve as a guide to the various techniques used to study surfaces. Purely optical techniques can be used to study interfaces under a wide variety of conditions.

Table 1-1. Overview of Surface Characterization Techniques, focusing on the type of information obtained and the limitations experienced.

Techniques	Information Obtained	Limitation
Contact Angle Goniometry	Hydrophilicity, hydrophobicity	Difficult to measure extremes from superhydrophilic (~0°) to superhydrophobic (>150°)
FTIR-GIR	Orientation/Conformation of molecules in monolayer/thin film	Substrate must be reflective (e.g. Au)
UV-Vis	Absorbance of film/monolayer (detect wavelength shift)	S/N may be low for monolayers/thin films
CFM	Imaging capability to detect film patterns	S/N may be low for monolayers/thin films; Use transparent substrate (e.g glass)
SPR	Changes in refractive index and chemical environment for biomolecules	Substrate needs to be metal (e.g. Ag, Au)
XPS	Atomic Composition, molecular conformation with multi-resolution spectra, thickness of film with ADXPS	Carbon contamination that can contribute to low S/N; Sample size needs to be 1 cm x 1 cm for most instruments
AFM/STM	Depth profiles, rms values	Substrate is highly recommended to be metal and needs to be extremely clean and stable
SEM	Morphology, roughness, patterns	Limited Resolution to micro-scale; Need conductive substrate
Ellipsometry	Thickness value and optical constant	Theory or model based
Xray Reflectivity	Density, chemical composition, thickness, and surface roughness	Intensity values are sensitive to defects on thin films

1.3.1 Contact Angle Goniometry

Contact Angle Goniometry is one of the most basic techniques used to measure the wettability of a surface.[24] Wettability basically refers to the attraction of a liquid to a solid substrate and is determined by the contact angle at which the liquid/vapor interface meets the solid surface. As shown in Figure 1-11, the contact angle meets at the intersection of three surface interactions – the solid liquid interfacial tension, γ_{SL}, liquid-vapor interfacial tension, γ_{LV}, and solid-vapor interfacial tension, γ_{SV}. Based on these surface interactions, a contact angle is an indication of how hydrophilic or hydrophobic a liquid is on a surface. A liquid is highly wettable on a given surface if the droplet spreads out on the substrate, but on a hydrophobic surface, the drop of liquid will ball-up and roll off the surface when tilted.

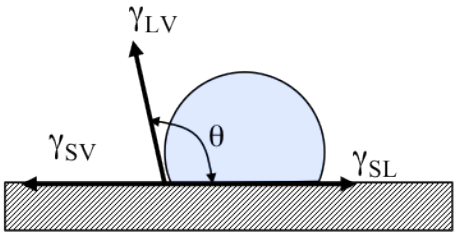

Figure 1-11. Contact Angle θ of a liquid on a surface that is dependent on the interactions between the interfacial tensions at the solid-liquid, solid-vapor, and liquid-vapor interfaces.

Contact angle goniometry is limited in its inability to accurately measure the extreme degrees of hydrophilicity and hydrophobicity. When the droplet completely spreads out on the solid surface, the contact angle will be close to 0°, thereby making the measurement more difficult. The other extreme on a highly hydrophobic surface is challenging as the liquid may bead off the surface too quickly to be measured. Furthermore, *static* contact angle measurements are limited by its assumption that the

surface is flat and rigid. In many cases where the surfaces are far from this ideal situation, *dynamic* contact angle measurements are used to measure additional features such as surface roughness with more advanced models.

1.3.2 Fourier Transform Infrared Grazing Incidence Reflection (FTIR-GIR) Spectroscopy

Fourier-Transform Infrared (FTIR) Spectroscopy is widely used to identify compounds, in particular their functional groups, by characteristic vibration modes within a defined spectral range. FTIR spectrometer can analyze samples via transmission, absorption and reflection. Reflection-based spectroscopy, referred to here as FTIR-Grazing Incidence Reflection (GIR) Spectroscopy, is advantageous in studying the chemical composition on surfaces. Polarization is used in GIR to determine the orientation of the molecules in a SAM by reflecting the IR beam off the surface at an angle between 80 and 88 degrees, as demonstrated in Figure 1-12. Isolating the perpendicular electric field provides information on the orientation of the transition moment in the SAM molecule – whether it is aligned with the electric field perpendicular or parallel to the plane of the substrate.

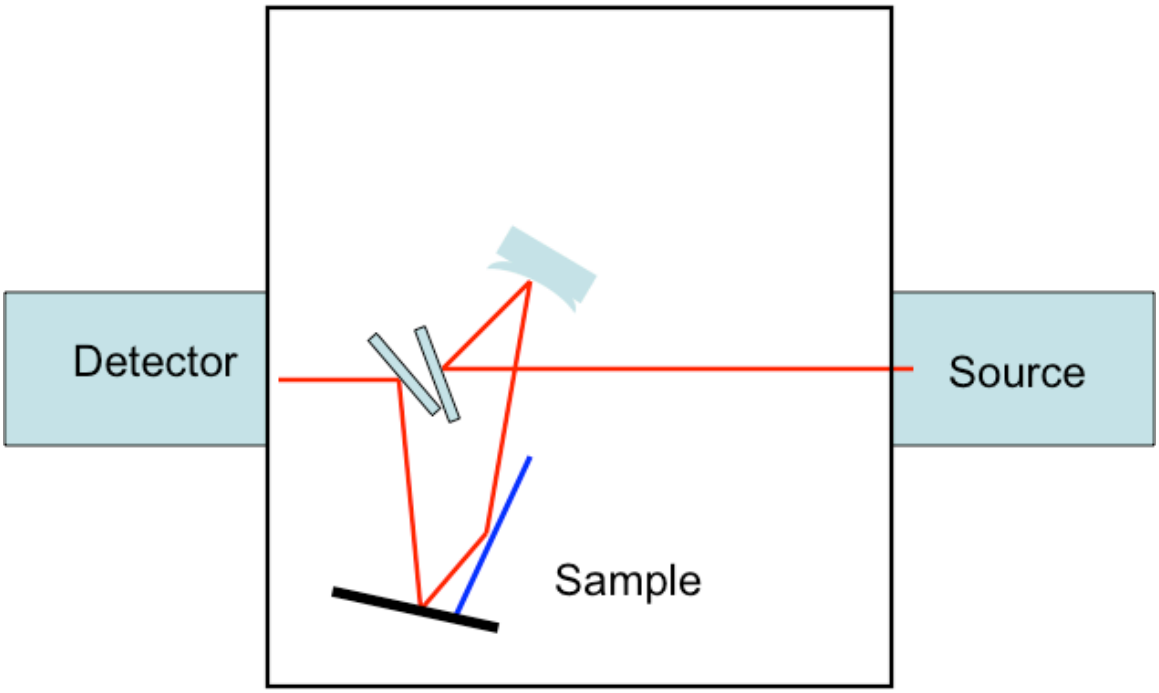

Figure 1-12. Grazing Incidence Reflection (GIR) Setup in FTIR Spectrometer. Red lines trace the IR beam path from the source to detector reflecting off the sample at an angle between 80 and 88 degrees.

Consequently, FTIR-GIR works particularly well with reflective surfaces such as gold, silver, or copper and exhibits poor signal-to-noise (S/N) ratio for non-reflective surfaces. The thin film/monolayer under spectral investigation can be as thin as 1 nm, which is a distinct advantage compared to other surface techniques. FTIR-GIR provides unique information on the orientation and conformation of the molecules composing the mono- and multi-layer films. The S/N ratio is typically low for monolayers, but a higher S/N can be reached with a functional group that has large absorption coefficient. For example, the carbonyl group, in the spectral range of 1700-1780 cm^{-1}, typically demonstrates a strong signal in the infrared spectrum. When the group more strongly couples with the perpendicular electric field that is isolated in FTIR-GIR spectroscopy, a stronger intensity of the peak is observed. The changes in absorption intensity of the

molecule's functional group can be used as a good indicator for molecular orientation on the surface in the form of a monolayer or thin film. It is known that the degree of chain ordering is dependent on the chain length and substrate quality.[13a]

1.3.3 Ultraviolet-Visible (UV-Vis) Spectroscopy

Ultraviolet-visible (UV-Vis) Spectroscopy uses light in the visible and adjacent ranges to analyze molecules that undergo electronic transitions and absorb light at a specific wavelength. UV-Vis is a quantitative measurement of different analytes that is typically carried out in solutions. With Beer-Lambert Law, the absorbance of a solution is used to calculate the concentration of the absorbing species in the solution and the path length. The wavelengths of the absorption peaks can be correlated with the types of bonds in a given molecule and are valuable in identifying the functional groups within a molecule. Any shift in wavelength is a good indicator of change in chemical composition of the molecule. While UV-Vis is typically used to analyze molecules in solution, there are modifications of this technique or sample handling that allows for analysis of molecules on surfaces in the form of monolayer or thin films. Monolayers or thin films that are immobilized onto a quartz substrate can be studied by UV-Vis because the quartz material allows the light to be transparent in this spectral region thereby not masking over the sample signal. However, UV-vis spectroscopy of a monolayer/thin film on quartz surfaces will be limited by weak S/N as the amount of material being analyzed is significantly lower than the bulk material studied in solution.

1.3.4 Confocal Fluorescence Microscopy (CFM)

Fluorescence Spectroscopy is a complementary technique to UV-Vis Spectroscopy that is used to analyze organic compounds in biochemical and medical

research fields. Fluorescence is an effective visual indicator particularly well used in imaging technology. Confocal Fluorescence Microscopy allows the ability to detect fluorescence from thin films and be able to improve signal-to-noise ratio by averaging up signals from different layers/slices taken by the CFM. The distinct advantage for CFM is the ability to image and detect patterns of fluorescence. However, one limitation of CFM is that the substrate needs to be transparent (e.g. glass or quartz) since CFM operates in transmission mode.

1.3.5 Surface Plasmon Resonance Spectroscopy (SPR)

SPR is one of the prevalent methods used in bio-diagnostic applications, particularly pertaining to the analysis of biomolecules interacting with a pre-functionalized surface in real time. SPR sensors are typically used to characterize conformational changes of protein molecules on surfaces by detecting changes in refractive indices and overall chemical environment. One distinct advantage is the ability to use SPR for in situ, real time measurements without the need for fluorescent tags. However, some drawbacks include the detection limit of low-concentration or low-molecular weight analytes as well as the need to use a metallic solid substrate.

1.3.6 X-ray Photoelectron Spectroscopy (XPS)

X-ray Photoelectron Spectroscopy (XPS) is a quantitative technique that characterizes surfaces by atomic composition. The spectroscopic technique works by bombarding the surface with a beam of X-rays and measuring the kinetic energy of electrons that escape from the top 1 to 10 nm of the material being analyzed. By varying the take off angle of the x-ray beam, XPS can be used to calculate the film thickness on the surface.

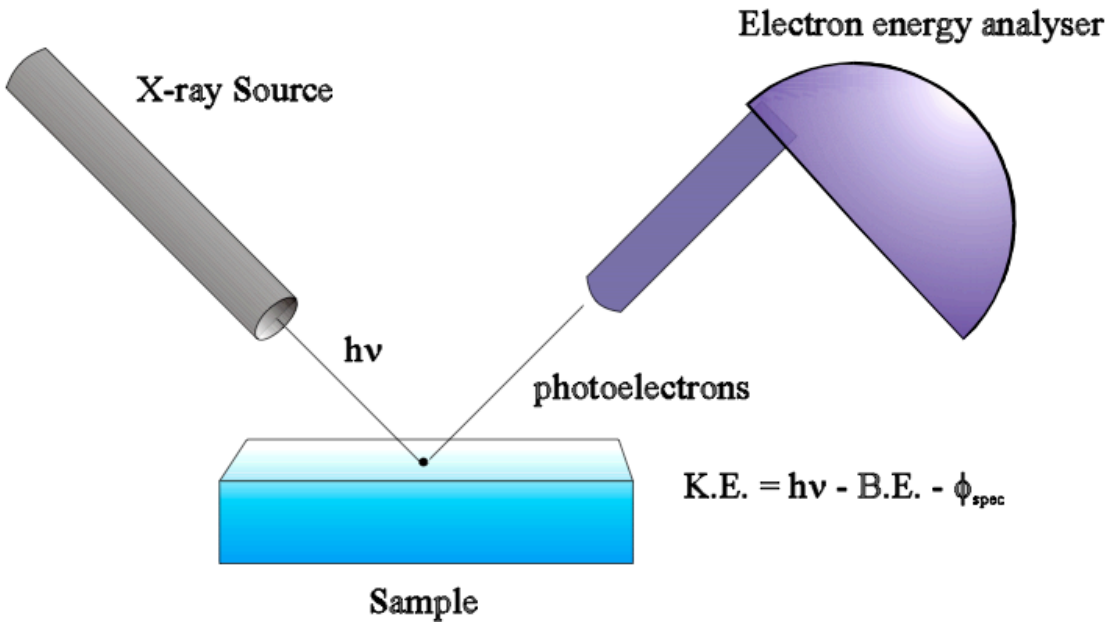

Figure 1-13. Schematic Illustration of how X-ray Photoelectron Spectroscopy operates.[25]

Furthermore, XPS can provide deep detail into the various chemical environments analyzed for a particular element in the film by exhibiting characteristic peaks. Older XPS instruments are limited to a small sample size (1×1 cm) and oversensitivity to contaminants on surfaces. In other words, the surfaces must be extremely clean for greatest accuracy.

1.3.7 Atomic Force Microscopy (AFM)/Scanning Tunneling Microscopy (STM)

Atomic Force Microscopy (AFM) is a high-resolution scanning probe that is capable of detecting films on a nano-scale. AFM offers valuable information in the form of images by "feeling" the surface with a mechanical probe composed of piezoelectric material. Through various modes from contact to non-contact, AFM produces micro and nano-scale features on the surface that is conveyed as a roughness factor. One of the

distinct advantages of the AFM is that the measurements can be taken in ambient conditions, similar to its counterpart, Scanning Tunneling Microscopy (STM).

STM can be used not only in ultra high vacuum but also in air, water and other liquid/gas ambients. STM is based on the concept of quantum tunneling as a conductive tip is brought very close to the surface in order to create a tunnel of electrons through the vacuum between them. By monitoring the current as the tip changes position across the surface, STM produces an image that offers similar information as that of AFM.

Both AFM and STM can be challenging because the techniques require extremely clean and stable surfaces, sharp tips, and excellent vibration control.

1.3.8 Scanning Electron Microscopy (SEM)

Scanning Electron Microscopy (SEM) images a sample by scanning it with a high-energy beam of electrons in a raster scan pattern. SEM offers information about the sample's surface topography, composition, and other properties such as electrical conductivity.

Due to the nature of how SEM operates, the technique is limited in the area of sample preparation. For conventional imaging, the sample must be electronically conductive at the surface and electronically grounded to prevent electrostatic overcharge. For metal samples, little sample preparation – cleaning and mounting properly onto the sample stage – is required for the SEM. However, nonconductive samples must be coated with an ultrathin coating of electrically conducting material, such as gold, by low vacuum sputter coating.

1.3.9 Ellipsometry

Ellipsometry is a non-destructive optical technique used to measure film thickness and optical constants of thin films.[26] This characterization technique is commonly used to characterize the film thickness for single and mulit-layers ranging from a few angstroms to nanometer with high accuracy. Spectroscopic ellipsometry measures the change of polarization in the measurement beam that is reflected from the sample. It faces limitations when the sample is not composed of well-defined layers that are optically homogeneous and isotropic. When these assumptions are violated, ellipsometry will not produce accurate results because the violated assumptions will invalidate the standard ellipsometric modeling procedure. The advantages of ellipsometric measurements, therefore, will be best demonstrated with samples that have discrete, uniform layers.

Ellipsometric measurements can also produce real time contrast images of the sample by using a CCD camera as a detector. Using a single-wavelength ellipsometer setup with a laser as a light source, the analysis of the measured data with computerized optical modeling leads to a deduction of spatially resolved film thickness. The images will provide information about the film thickness and refractive index and will be complimentary in detecting patterns on thin films.

1.3.10 X-ray Reflectivity (XRR)

X-ray Reflectivity is a surface-sensitive technique used to characterize monolayers and thin films on surfaces that is complementary to ellipsometry. XRR is a non-destructive, commonly used technique to estimate density, thickness and roughness of thin films on a nano-scale. The technique is based on total external reflection of X-

rays on surfaces and interfaces. XRR can be used to analyze amorphous, crystalline and liquid samples. The technique can measure a layer thickness ranging from 5 Angstroms to 400 nm and surface roughness ranging from 0 to 20 Angstroms.

Deviations from the law of Fresnel reflectivity are analyzed to obtain a density profile of the interface normal to the surface as a beam of x-rays is reflected off the surface under investigation. Through optimized reflectivity experiments, the specular reflectivity and large features characterizing the sample (e.g. Bragg's peak, Kiessig oscillations) are detected.

XRR is limited when the sample shows no difference in electron density between layers and with substrate. There are further limitations with defects in thin films as XRR intensity values are very sensitive to inconsistent changes in roughness.

1.4 Thesis Overview

This thesis ties the fundamental study of a photoactive monolayer with its direct biomedical applications in grafting nanoparticles to the surface. Chapter 2 covers a multi-faceted spectroscopic investigation of the phthalimide-thiol SAM and its similar molecular systems to answer fundamental questions of monolayer organization. The application of a photoactive monolayer to graft nanoparticles onto a surface will be the topic of Chapter 3. The final chapter will introduce the study of oysters and its ability to filter heavy metals, as a result of my collaboration with Harbor High School and Brookhaven National Laboratory through the NSF GK-12 Fellowship.

1.5 References

1. Miozzo, L.; Yassar, A.; Horowitz, G., Surface Engineering for high performance organic electronic devices: the chemical approach. *J. Mater. Chem.* **2010,** *20*, 2513-2538.

2. Ito, Y., Photoimmobilization for Microarrays. *Biotechnol. Prog.* **2006,** *22*, 924-932.

3. Nuzzo, R. G.; Allara, D. L., Adsorption of bifunctional organic disulfides on gold surfaces. *J. Am. Chem. Soc.* **1983,** *105*, 4481-4483.

4. Porter, M. D.; Bright, T. B.; Allara, D. L.; Chidsey, C. E. D., Spontaneously Organized Molecular Assemblies. 4. Structural Characterization of n-Alkyl Thiol Monolayers on Gold by Optical Ellipsometry, Infrared Spectroscopy, and Electrochemistry. *J. Am. Chem. Soc.* **1987,** *109*, 3559-3568.

5. (a) Somorjai, G. A., *Chemistry in Two Dimensions: Surfaces*. Cornell University Press: Ithaca, NY, 1981; (b) Durand, R. R.; Bencosme, C. S.; Collman, J. P.; Anson, F. C., Mechanistic aspects of the catalytic reduction of dioxygen by cofacial metalloporphyrins. *J. Am. Chem. Soc.* **1983,** *105*, 2710-2718.

6. Carroll, G. T.; Wang, D.; Turro, N. T.; Koberstein, J. T., Photochemical Micropatterning of Carbohydrates on a Surface. *Langmuir* **2006,** *22*, 2899-2905.

7. (a) Langmuir, I., The Constitution and Fundamental Properties of Solids and Liquids. II. Liquids. *J. Am. Chem. Soc.* **1917,** *39*, 1848-1906; (b) Blodgett, K. B., Films Built by Depositing Successive Monomolecular Layers on a Solid Surface. *J. Am. Chem. Soc.* **1935,** *57*, 1007-1022.

8. Bigelow, W. C.; Pickett, D. L.; Zisman, W. A., Oleophobic Monolayers. I. Films Adsorbed From Solution in Non-Polar Liquids. *J. Colloid Sci.* **1946,** *1*, 513-538.

9. Sagiv, J., Organized Monolayers by Adsorption. 1. Formation and Structure of Oleophobic Mixed Monolayers on Solid Surfaces. *J. Am. Chem. Soc.* **1980,** *102*, 92.

10. Allara, D. L.; Nuzzo, R. G., Spontaneously Organized Molecular Assemblies. 1. Formation, Dynamics, and Physical-Properties of Normal-Alkanoic Acids Adsorbed From Solution On an Oxidized Aluminum Surface. *Langmuir* **1985,** *1*, 45-52.

11. Nuzzo, R. G.; Zegarski, B. R.; Dubois, L. H., Fundamental Studies of the Chemisorption of Organosulfur Compounds on Au(111). Implications for Molecular Self-Assembly on Gold Surfaces. *J. Am. Chem. Soc.* **1987,** *109*, 733-740.

12. Park, E. J.; Carroll, G. T.; Koberstein, J. T.; Turro, N. T., Shedding light on Surfaces - using photons to transform and pattern material surfaces. *Soft Matter* **2009,** *5*, 36-50.

13. (a) Vericat, C.; Vela, M. E.; Benitez, G.; Carro, P.; Salvarezza, R. C., Self-assembled monolayers of thiols and dithiols on gold: new challneges for a well-known system. *Chem. Soc. Rev.* **2010,** *39*, 1805-1834; (b) Badia, A.; Lennox, R.; Reven, L., A Dynamic View of Self-assembled Monolayers. *Acc. Chem. Res.* **2000,** *33*, 475-481; (c) Himmelhaus, M.; Eisert, F.; Buck, M.; Grunze, M., Self-assembly of n-Alkanethiol Monolayers. A Study by IR-Visible Sum Frequency Spectroscopy (SFG). *J. Phys. Chem. B* **2000,** *104*, 576-584.

14. Ulman, A., Formation and Structure of Self-Assembled Monolayers. *Chem. Rev.* **1996,** *96*, 1533-1554.

15. (a) Godin, M.; Williams, P. J.; Tabard-Cossa, V.; Laroche, O.; Beaulieu, L. Y.; Lennox, R. B.; Grutter, P., Surface Stress, Kinetics, and Structure of Alkanethiol Self-Assembled Monolayers. *Langmuir* **2004,** *20*, 7090-7096; (b) Calvente, J. J.; Lopez-Perez,

G.; Jurado, J. M.; Andreu, R.; Molero, M.; Roldan, E., Reorientation of Thiols during 2D Self-Assembly: Interplay between Steric and Energetic Factors. *Langmuir* **2010,** *26*, 2914-2923.

16. (a) Wang, Y.; Zhou, Y.; Sokolov, J.; Rigas, B.; Levon, K.; Rafailovich, M., A potentiometric protein sensor built with surface molecular imprinting method. *Biosens. Bioelectron.* **2008,** *24*, 162-166; (b) Chen, H.; Heng, C. K.; Puiu, P. D.; Zhou, X. D.; Lee, A. C.; Lim, T. M.; Tan, S. N., Detection of Saccharomyces cerevisiae immobilized on self-assembled monoalyer (SAM) of alkanethiolate using electrochemical impedance spectroscopy. *Anal. Chim. Acta* **2005,** *554*, 52-59; (c) Huang, T. J.; Brough, B.; Ho, C.-M.; Liu, Y.; Flood, A. H.; Bonvallet, P. A.; Tseng, H.-R.; Stoddart, J. F.; Baller, M., A nanomechanical device based on linear molecular motors. *Appl. Phys. Lett.* **2004,** *85*, 5391-5393.

17. Rengifo, H. R.; Chen, L.; Grigoras, C.; Ju, J.; Koberstein, J. T., "Click-Functional" Block copolymers provide precise surface functionality via spincoating. *Langmuir* **2008,** *24*, 7450.

18. Reiter, G.; de Gennes, P. G., Spin-cast, thin, glassy polymer films: highly metastable forms of matter. *Eur. Phys. J. E.* **2001,** *6* (1), 25-28.

19. Rozsnyai, L. F.; Fodor, S. P. A.; Schultz, P. G.; Benson, D. R., Photolithographic immobilization of biopolymers on solid supports. *Angew. Chem.* **1992,** *104* (6), 801-802.

20. Pease, A. C.; Solas, D.; Sullivan, E. J.; Cronin, M. T.; Holmes, C. P.; Fodor, S. P. A., Light-generated oligonucleotide arrays for rapid DNA sequence analysis. *Proc. Natl. Acad. Sci. U.S.A.* **1994,** *91* (11), 5022-5026.

21. Wang, Y.; Zhong, W.; Jiang, N.; Yang, W., Directly Fabricating Monolayer Nanoparticles on a Polymer Surface by a UV-Induced MMA/DVB Microemulsion Graft Polymerization. *Macromol. Rapid Commun.* **2005,** *26*, 87-92.

22. (a) Delamarche, E.; Sundarababu, G.; Biebuyck, H.; Michel, B.; Gerber, C.; Sigrist, H.; Wolf, H.; Ringsdorf, H.; Xanthopoulos, N.; Mathieu, H. J., Immobilization of Antibodies on a Photoactive Self-Assembled Monolayer on Gold. *Langmuir* **1996,** *12*, 1997-2006; (b) Prucker, O.; Naumann, C. A.; Ruhe, J.; Knoll, W.; Frank, C. W., Photochemical Attachment of Polymer Films to Solid Surfaces via Monolayers of Benzophenone Derivatives. *J. Am. Chem. Soc.* **1999,** *121* (38), 8766-8770; (c) Hasegawa, M.; Matano, T.; Shindo, Y.; Sugimura, T., Spontaneous Molecular Orientation of Polyimides Induced by Thermal Imidization 2. In-Plane Orientation. *Macromolecules* **1996,** *29*, 7897-7909; (d) Dormán, G.; Prestwich, G. D., Benzophenone Photophores in Biochemistry. *Biochemistry* **1994,** *33* (19), 5661-5673; (e) Dormán, G.; Prestwich, G. D., Using Photolabile Ligands in Drug Discovery and Development. *Trends in Biotechnology* **2000,** *18*, 64-77; (f) Jeyaprakash, J. D.; Samuel, S.; Ruhe, J., A Facile Photochemical Surface Modification Technique for the Generation of Microstructured Fluorinated Surfaces *Langmuir* **2004,** *20*, 10080-10085.

23. Kanaoka, Y., Photoreactions of Cylic Imides. Examples of Synthetic Organic Photochemistry. *Acc. Chem. Res.* **1978,** *11* (11), 407-413.

24. de Gennes, P. G., Wetting: statics and dynamics. *Rev. Mod. Phys.* **1985,** *57*, 827-863.

25. Wikipedia, X-ray Photoelectron Spectroscopy. Wikipedia Foundation, Inc.: 2011.

26. Fujiwara, H., *Spectroscopic Ellipsometry: Principles and Applications*. John Wiley & Sons, Ltd: West Sussex, England, 2007.

2 Fundamental Study of Phthalimide Monolayers and Thin Films

2.1 Introduction: Monolayers and Thin Films

Self-assembled monolayers (SAMs) of organic molecules have been deposited on various types of substrates and been extensively studied due to their strong potential applications ranging from nanotechnology fabrication techniques to surface coatings on biomedical devices.[1] Studies have attempted to answer fundamental questions on the nature of the interactions of the monolayer with the substrate, and the thermodynamics of the self-assembly process and how the molecules interact with each other as they spontaneously organize into a film. Fabricating monolayers with well-defined composition, order, and thickness has important implications from a fundamental and technological standpoint.

It is recognized that the formation of an alkanethiol SAM involves a sequence of several structural phase transitions with varying degree of surface coverage. In the lower coverage arrangement, Scanning Tunneling Microscopic topographs[2] suggest that the alkanethiols are oriented parallel to the Au surfaces. While the molecules are oriented in a stacked lying-down phase with modest coverage, the alkanethiols in the greater coverage area are expected to be in the standing-up phase in which the molecules are oriented (semi-) perpendicular to the substrate. These phase transitions help us understand that the self-assembly process depends on the length of immersion time, the solvent choice, temperature conditions, and other variables, thereby determining the overall structure of the resulting monolayer.[2a, 3]

The self-assembly sequence has been first introduced in Chapter 1, but will be further explored in this chapter (Figure 2-1). In the first stage, the SF group chemisorbs onto the gold substrate. Second step, once the molecule is anchored down, the molecule may initially be in the lying down phase, then orients itself upright perpendicular to the substrate (Figure 2-1A).[4] Lastly, as more molecules adsorb onto the surface, the alkyl chains detangle and gradually, the packing density of monolayer increases (Figure 2-1B). The resulting monolayer leaves a certain functional group exposed at the air-monolayer interface once the surface is taken out of solution and dried (Figure 2-1C).

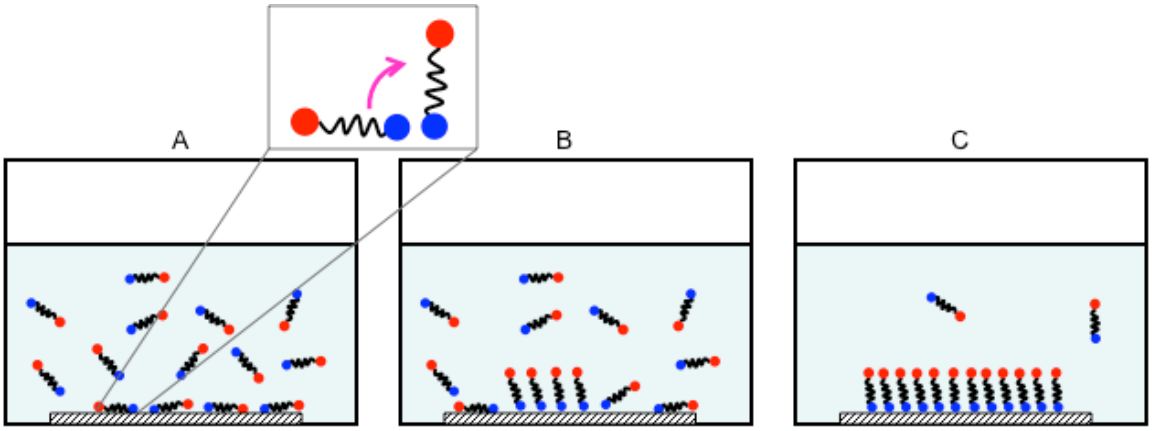

Figure 2-1. Schematic illustration of self-assembly process.

Of all the monolayers studied, alkanethiol monolayers are probably the most well known. As illustrated in Figure 2-2, each component of an alkanethiol molecule in the monolayer is characterized by energy in varying orders of magnitude that dictate the self-assembly process, SF-substrate interaction being the strongest at 50 kcal/mol for thiolate-Au bond formation. SP-SP interactions value at a mere 1-2 kcal/mol, but these van der Waals interactions cannot be underestimated because many of them together have the authority to govern the ordering of a monolayer. Also, with regards to the stability against oxidation and thermal desorption of the thiol compounds adsorbed on gold

surfaces, it is important to find a way to control the chemistry and structure of SAMs. The search for strategies to increase oxidation resistance of SAMs has greater weight for their use in ambient conditions. The fact that SAMs are only stable up to to 100°C is a serious concern.

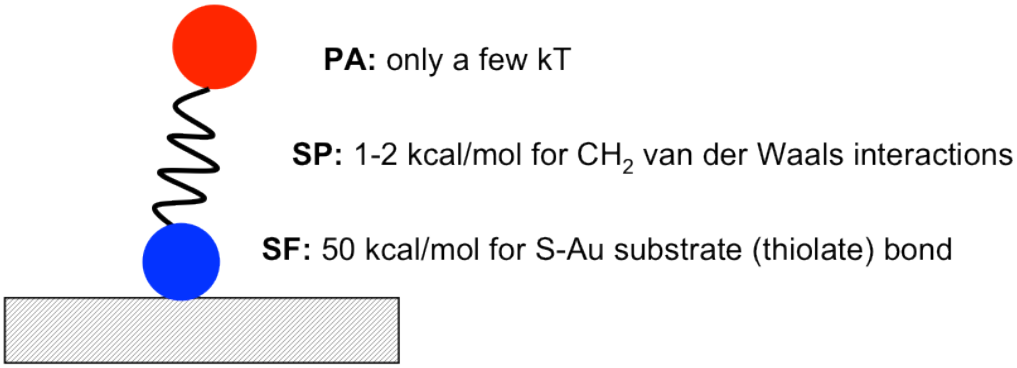

Figure 2-2. Monolayer composed of Alkanethiol molecules and respective energies for each component.[5]

Even after thousands of years of studying alkanethiol SAMs, there is still some controversy over the basic concepts of thiol SAMs related to the following: the chemistry of alkanethiolate-Au bond in SAMs, control over the quality of SAMs, and the structure of monolayer at air-adsorbate interface. We will discuss the last topic mentioned with a particular focus on a photoactive moiety. Monolayers with phthalimide terminal groups will be closely investigated in this thesis. The structure and orientation of these molecules have been studied on glass substrates.[6]

2.1.1 *N*-Phthalimide-heptadecyl-trichlorosilane Monolayer on Glass/Silicon

(*N*-Phthalimidoheptadecyl)trichlorosilane was self-assembled onto glass/silicon substrate to produce a pure phthalimide monolayer (P-SAM). P-SAMs were compared to mixed monolayers with hexadecyltrichlorosilane (HTS) by thorough spectroscopic

analysis (Figure 2-3). XPS and FTIR Spectroscopy results provided enough information to calculate the surface coverage and orientation of the molecules on the surface.

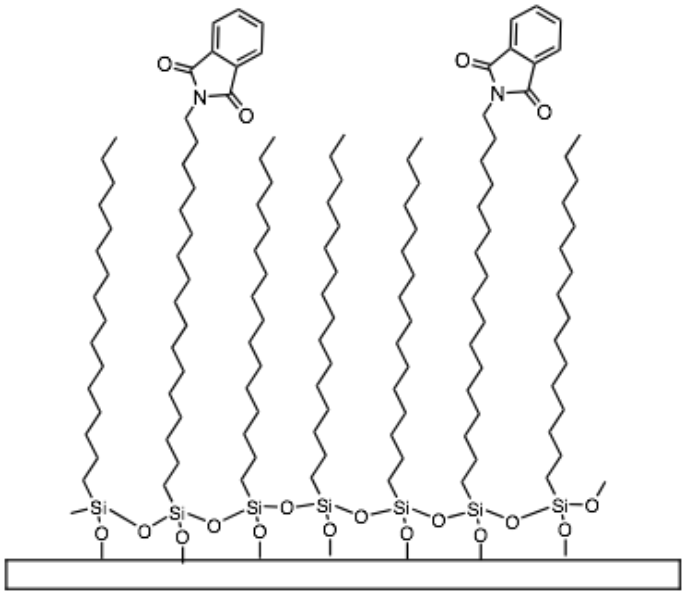

Figure 2-3. Mixed Monolayer of N-Phthalimidoheptadecyl-trichlorosilane (PHTS) and Hexadecyltrichlorosilane (HTS).[6]

Heid et. al.[6] calculated the surface coverage of pure P-SAM to be 62.5%. The low surface coverage of pure P-SAM can be explained by two reasons. First, the low surface coverage indicates a nonhomogeneous orientation of the molecules in the monolayer. The other likely possibility is that the steric or repulsive dipole-dipole interactions between the phthalimide terminal groups hindered the molecules from densely packing. To counteract such forces, researchers have prepared mixed monolayers of PHTS and HTS to produce films with higher surface coverage. The mixed SAMs produced a surface coverage as high as 96.0% with a PHTS:HTS mixture ratio of 1:19. The lowest surface coverage produced was 71.8% with a mixture ratio of 1:1, but still higher than that of pure P-SAMs. As observed in Figure 2-3, the HTS molecules act as fillers in between the phthalimide molecules that are spaced apart from each other to minimize any

steric or repulsive forces. It is interesting to note the surface coverage differences of this pure P-SAM on glass, compared to the mixed SAMs, because it will help us understand our phthalimide-undecyl-thiol SAMs on gold substrates as will be discussed in this chapter.

2.1.2 Phthalimide-undecyl-thiol Monolayer on Gold

Phthalimide-undecyl-thiol, referred to as molecule **1**, is studied in the form of monolayers and thin films on gold substrates (Figure 2-4). The terminal group exposed at the air-monolayer interface plays a crucial role in defining the surface chemistry. If the surface was functionalized with a phthalimide monolayer, the photoactive moiety holds the power to anchor various molecules, biomolecules, or nanostructures by strong covalent bond attachments.[7] Furthermore, the key to controlling surface reactivity is to understand the orientation of the terminal group with respect to the rest of the molecule and to the substrate, as dictated by angles α, β, and χ (Figure 2-4).

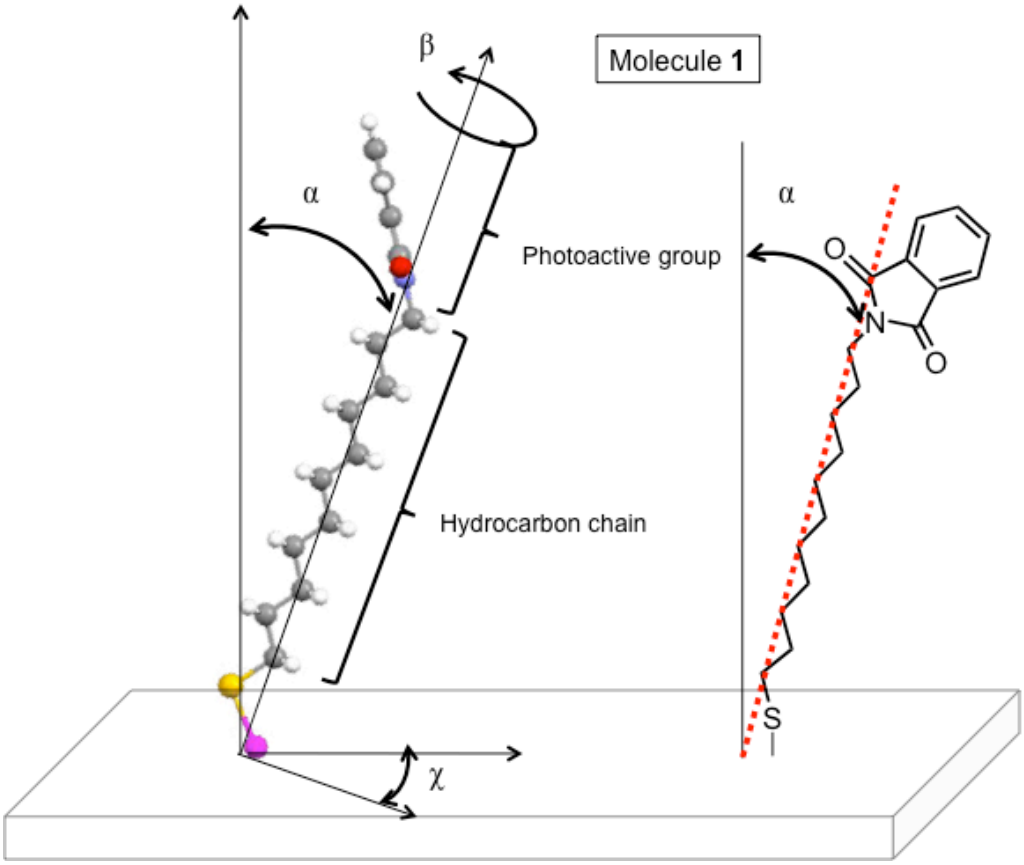

Figure 2-4. Scheme of molecule 1 (phthalimide-undecyl-thiol) adsorbed onto the surface of a Au substrate in a standing up conformation. Typical angles are α, β, and χ; Pink: Gold atom; Yellow: Sulfur atom; Gray: Carbon atom; White: Hydrogen atom. Red: oxygen atom; Purple: Nitrogen atom.

There are two factors that affect the photo-reactivity of the phthalimide-undecyl-thiol SAM on Au substrate. First, the organization and density of the SAM will determine whether the phthalimide functional group will have poor or strong reactivities at the air-monolayer interface. Results suggest that functional groups positioned within highly ordered organic interfaces can have poor reactivities.[7] Secondly, the position of reactive sites is important. Reaction sites positioned below the surface of the SAM or "embedded" in the SAM can be less accessible to reactants in the surrounding medium

than the ones positioned at the termini of the SAM.[8] In mixed SAMs, steric effect is reduced and consequently, the reactive site may be more accessible.

In this thesis, we will not demonstrate the reactivity of the phthalimide SAM, but rather study the structure of the static monolayer. Future work, however, should investigate the photo-dynamics of the phthalimide SAM. In order to understand the behavior of a monolayer of **1**, we prepared multi-layer films that were deposited via spin-coating. Therefore, it is essential to learn more about the process of spin-coating and how that would affect the structure/composition of the formed film.

2.2 Methods

2.2.1 Materials

Sodium thiophosphate decahydrate (purchased from VWR), Potassium Phthalimide (purchased from Sigma-Aldrich), Dimethylformamide (DMF; purchased from Sigma-Aldrich), Tetrahydrofuran (THF; purchased from Sigma-Aldrich), Sulfuric acid (purchased from Sigma-Aldrich), and hydrogen peroxide (purchased from VWR) were used as received. Gold-coated microscope slides (25.4 mm × 76.2 mm × 1.5 mm, with 100 nm Au film on a 10 nm Ti adhesion layer; Evaporated Metal Films, Inc.) were used for monolayer deposition.

2.2.2 Synthesis of Molecule 1, Phthalimide-undecyl-thiol[9]

Phthalimide-undecyl-bromide (1.0 equiv) and sodium thiophosphate (1.0 equiv) were dissolved in a water/DMF mixture. The reaction mixture was stirred overnight at room temperature. The pH was lowered to 4.0 with 3.5% HCl and the reaction was stirred overnight. The reaction mixture was extracted with methylene chloride (3x) and washed with brine, then dried over $MgSO_4$ and filtered under vacuum to yield a white crystalline solid product.

2.2.3 Gold Substrate Cleaning

Gold substrates for FTIR-GIR were used as provided by EMF Inc. Immediately prior to monolayer modification the Au substrates were cleaned in a freshly prepared "piranha" solution for two hours at room temperature (Caution: a "piranha" solution, 1:2 concentrated H_2SO_4/30% H_2O_2, reacts violently with many organic materials and should

be used with extreme caution; it should not be stored in sealed containers), rinsed with deionized water and ethanol, and then dried in a flowing stream of Ar.

2.2.4 Sample Preparation

Self-Assembled Monolayers of Phthalimide-undecyl-thiol (A). Monolayers were prepared by immersing clean gold substrates overnight in 1 mM phthalimide-undecyl-thiol dissolved in THF. Substrates were rinsed with ethanol and water, then dried with Ar.

Preparation of Spincoated sample (B). Sample B was prepared by dropping 1 mM phthalimide-undecyl-thiol (in THF) solution onto substrate as it was spinning at a rate of 200 rpm for 1 min.

Preparation of Annealed/Spincoated Sample (C). Sample C was prepared by heating the spincoated samples at 80°C for 30 minutes. Rinsed with ethanol and water, three times, and then dried with Argon gas.

Isotropic Sample (1). The phthalimide-undecyl-thiol solid sample was placed onto an Attenuated Total Reflectance (ATR) ZnSe crystal to obtain the bulk FTIR spectrum.

2.2.5 Instrumentation

FTIR spectra were obtained using a Thermo Nexus 570 interferometer with a globar, a KBr beam splitter, and a DTGS detector. The isotropic sample as a crystalline solid was analyzed with Attenuated Total Reflection (ATR - 256 scans, a resolution of 4 cm^{-1}, equipped with ATR unit from Thermo). Thin film samples (Samples **A**, **B**, and **C**) were characterized by FTIR-GIR spectroscopy (Nexus 570 FTIR interferometer with a globar element focused onto the apex of the plane mirror/monolayer support at an angle

of 85° as shown in Figure 2-5). An average of 150 scans at a resolution 4 cm^{-1} were collected in nitrogen-purged conditions.

Raman spectra were collected using a LabRam ARAMIS Raman Microscope from HORIBA Jobin Yvon with a 532 nm laser, no filter, 2 second/acquisition, 50 scans, centered grating at 1800 cm-1 with 600 grating.

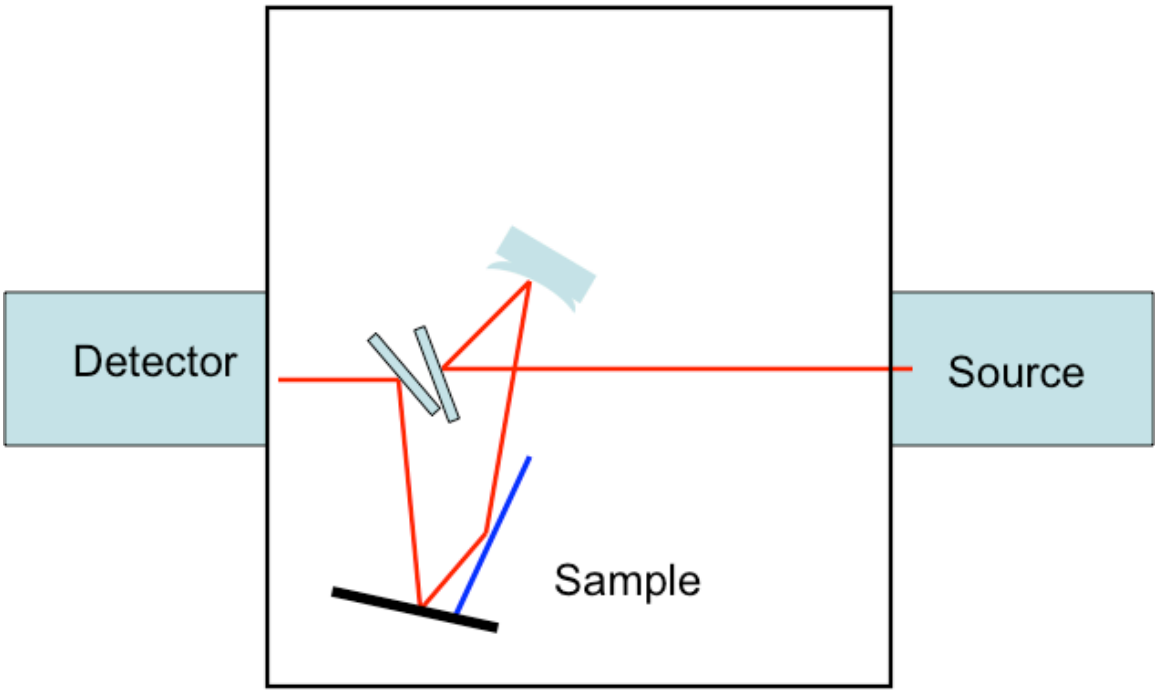

Figure 2-5. Schematic illustration of grazing incidence reflection setup in FTIR instrument using a modified Harrick attachment.

X-ray photoelectron spectroscopy (XPS) spectra were recorded with a PHI 5500 model spectrometer equipped with an Al Kα monochromator X-ray source run at 15 kV and 23.3 mA, a hemispherical electron energy analyzer, and a multichannel detector. The test chamber pressure was maintained below 2×10^{-9} Torr during spectral acquisition. A low-energy electron flood gun was used to neutralize the possible surface charge. The XPS binding energy (BE) was internally referenced to the aliphatic C(1s) peak (BE = 284.6 eV). Survey spectra were acquired at an analyzer pass energy of 93.9 eV and BE

resolution of 0.8 eV, while high-resolution spectra were acquired with a pass energy of 23.5 eV and BE resolution of 0.05 eV. The takeoff angle is defined as the angle between the surface normal and detector. Angle-dependent XPS (ADXPS) was performed by using a motor to rotate sample holder to the desired takeoff angle. A PHI data processing software package was used to subtract the background of high-resolution spectra and the spectra were resolved by fitting each peak with Gaussian-Lorentz functions under the constraint of setting a reasonable BE shift and characteristic full width of half-maximum range.

2.3 Results and Discussion

2.3.1 Characterization of Molecule 1

The synthesis of **1** and analogs have been reported in literature and followed accordingly.[9] FTIR-ATR and Raman spectroscopic results demonstrate characteristic peaks of **1**, particularly the imide carbonyl and methylene stretching modes (Figure 2-6). The imide carbonyl stretches demonstrate the expected differences in intensity between the Raman and IR results. The symmetric C=O stretch at 1771 cm^{-1} is Raman active while it is IR inactive at 1768 cm^{-1}. The stronger Raman intensity is due to polarizability changes during vibration that allows strong Raman light scattering (Raman active). Similarly, the asymmetric C=O stretch at 1710 cm^{-1} is Raman inactive while molecule **1** produces a strong signal in the infrared. In the asymmetric stretch, the electrons are more easily polarized in the bond that expands but are less easily polarized in the bond that compresses. As a result, there is no overall change in polarizability and asymmetric stretch is Raman inactive at 1710 cm^{-1}. Mass Spectroscopy confirms the molecular mass of **1** as 333 g/mol.

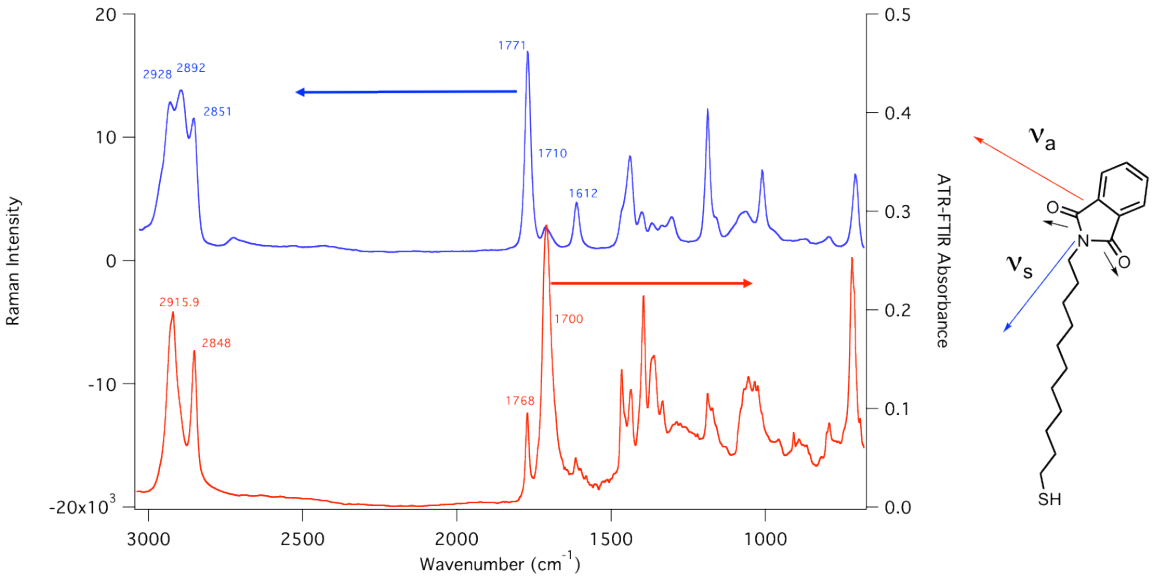

Figure 2-6. FTIR-ATR and FT-Raman Spectroscopic characterization of 1.

2.3.2 FTIR-GIR Spectra of pure SAM and Thin films of 1

FTIR Spectroscopy can identify a variety of substances by characteristic vibration frequencies, but its ability to provide comprehensive analysis is dependent on the type of sample analyzed and accessory used. In this case, the samples are thin films on gold surfaces, which pose some challenges including difficulty in detecting a good signal-to-noise (S/N) level. Grazing Incidence Reflection (GIR) accessory (Section 1.3.2) can address this challenge and collect high S/N ratio from nanometer-thin layers on reflective surfaces. FTIR-GIR is able to identify functional groups of the adsorbate, but also determine the molecular orientation on the surface. GIR accessory is a good candidate for the type of analysis desired for SAM and multilayer films of **1** on gold surfaces. By grazing the infrared beam off the gold surface at an angle of 80-88 degrees, we are able to isolate the electric field perpendicular to the surface, detect the functional groups that are more strongly coupling to the electric field, and determine the overall orientation of the adsorbate on the surface (See Figure 2-7). In particular, molecule **1** has its advantage of

being well marked by carbonyl groups, which possess strong absorption coefficient in the infrared region.

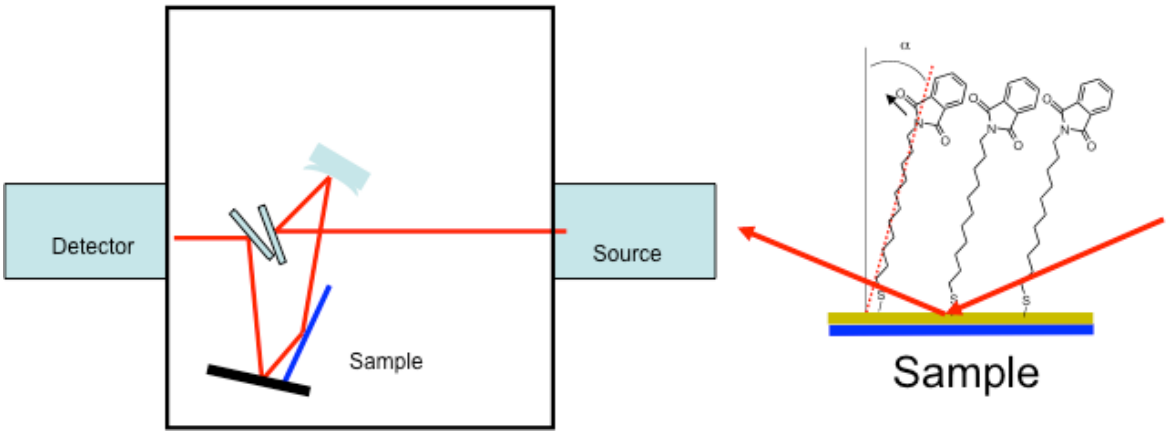

Figure 2-7. Schematic illustration on the right shows the path of the infrared beam off gold substrate.

In addition to tracking the carbonyl functionality of molecule **1** on the surface, we can identify methylene groups and will study both functional groups for all samples. Samples under investigation are (A) Self-assembled Monolayer, (B) Spin-coated thin film, and (C) Annealed/Spin-coated thin film of **1**.

2.3.2.1 C-H and C=O Stretching Frequencies

The relative GIR spectral change of the monolayer and thin films was used to determine the chemical bonding and molecular orientation of **1** at the interface region on gold substrates. Figure 2-8 shows the comparison of four infrared spectra in the C-H and C=O stretching regions: one ATR spectrum of the isotropic sample, **1** and GIR spectra of samples **A**, **B,** and **C**. No significant differences can be seen in these spectra in terms of the total number of bands. However, the relative band intensities are quite different. As seen in Figure 2-8, in the 3000–2700 cm^{-1} region, the C–H stretching bands, there are significant differences in the relative intensity of the bands and there are wavenumber

shifts that can be attributed to the change of the alkyl chain order on the surface. Molecule **1** in bulk, a crystalline state, demonstrates order as the asymmetric and symmetric methylene stretches are positioned at 2916 cm^{-1} and 2848 cm^{-1}, respectively.[10] Interestingly, when **1** adsorbs onto a gold surface (i.e. samples **A**, **B**, or **C)**, we observe the methylene peaks to shift significantly to higher wavenumbers (Table 2-1).

The sharp and intense bands at 1774 and 1720 cm^{-1} on Samples **A**, **B**, and **C** are attributed to the C=O symmetric and asymmetric stretching modes of the phthalimide terminal group, respectively (Table 2-1). These bands in an isotropic form have been reported in the literature by Rigout, M. et. al.[11] The shift to higher wavenumber for both methylene and carbonyl groups is an indication of disorder in the monolayer/films, and could be due to low surface coverage.[12]

The characteristic S–H stretching mode of the thiol group at 2571 cm^{-1} is not observed in the isotropic spectrum. This absence is plausibly due to the easily oxidized thiol end groups in the isotropic medium, which can come together to generate a cystine unit with a disulfide bond (-S–S-). In the GIR spectra, the absence of this S–H peak on the gold surface is expected as the thiol group interacts with gold to form a S-Au bond.

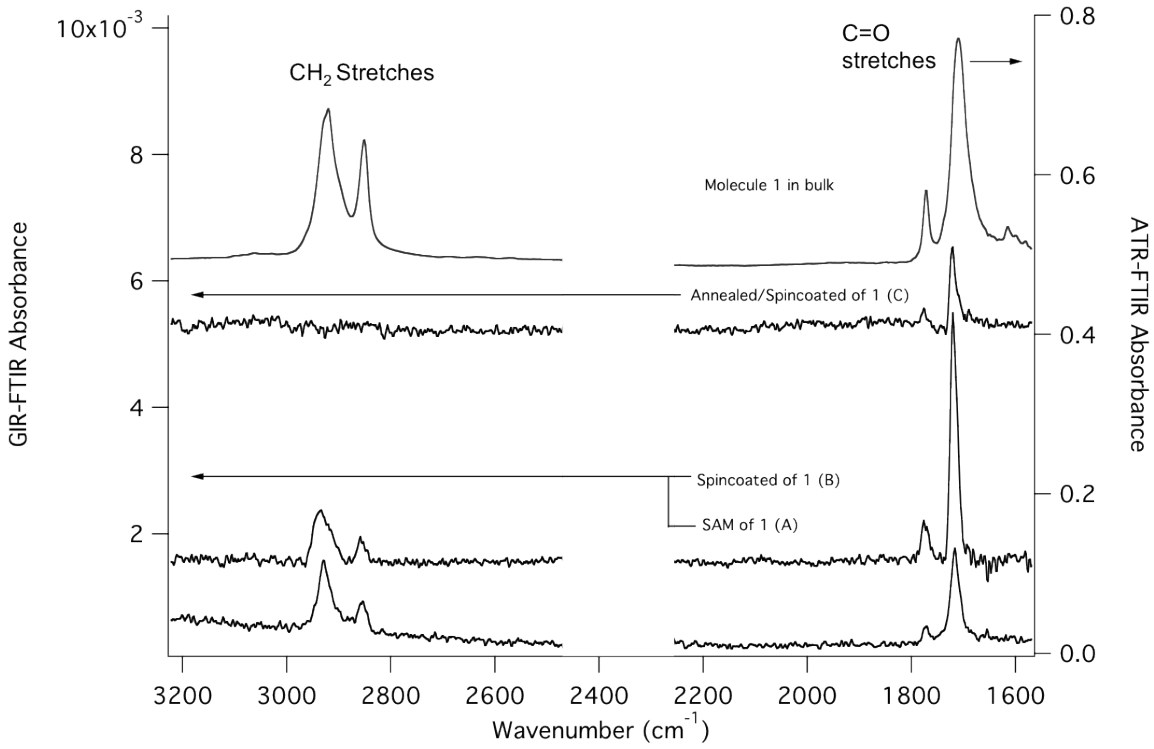

Figure 2-8. Fourier Transform Infrared Grazing Incidence Reflection (FTIR-GIR) Spectroscopy of SAM of 1 (A), Spincoated of 1 (B), and Annealed/Spincoated of 1 (C), which is scaled with the left axis while the bulk spectrum of 1 is scaled with respect to the right axis. Carbon dioxide gas was observed in the spectra but covered for easier view.

Table 2-1. Peak Positions (cm^{-1}) Molecule 1 in Crystalline State and Adsorbed onto Gold Surfaces

Sample	*Asymmetric Methylene (CH_2)*	Symmetric Methylene (CH_2)	Symmetric Phthalimide (C=O)	*Asymmetric Phthalimide (C=O)*
Molecule **1** (bulk)	2916	2848	1768	1700
SAM of **1** (**A**)	2929	2854	1774	1720
Spincoated of **1** (**B**)	2937	2854	1774	1720
Annealed/Spincoated of **1** (C)	No peak	No peak	1774	1720

2.3.2.2 C-H and C=O Absorbance Intensities

The stretching frequency alone will not determine the state of disorder or order of the monolayer and films. Since the stretching frequency of carbonyls has not changed from being in bulk to surface conformation, we will evaluate the absorbance intensities of carbonyl groups because the intensity change is a good indication of how the molecule is oriented on the substrate. As Figure 2-9 illustrates, there are two stretching modes associated with the phthalimide carbonyl group – asymmetric ν_a and symmetric ν_s. When the two carbonyl groups on the phthalimide stretch symmetrically, the peak appears at 1774 cm^{-1}. When the imide carbonyls vibrate disproportionately, they produce an asymmetric frequency at 1720 cm^{-1}. As expected, the asymmetric vibration is stronger in intensity than the symmetric vibration as shown in Figure 2-9 (left).

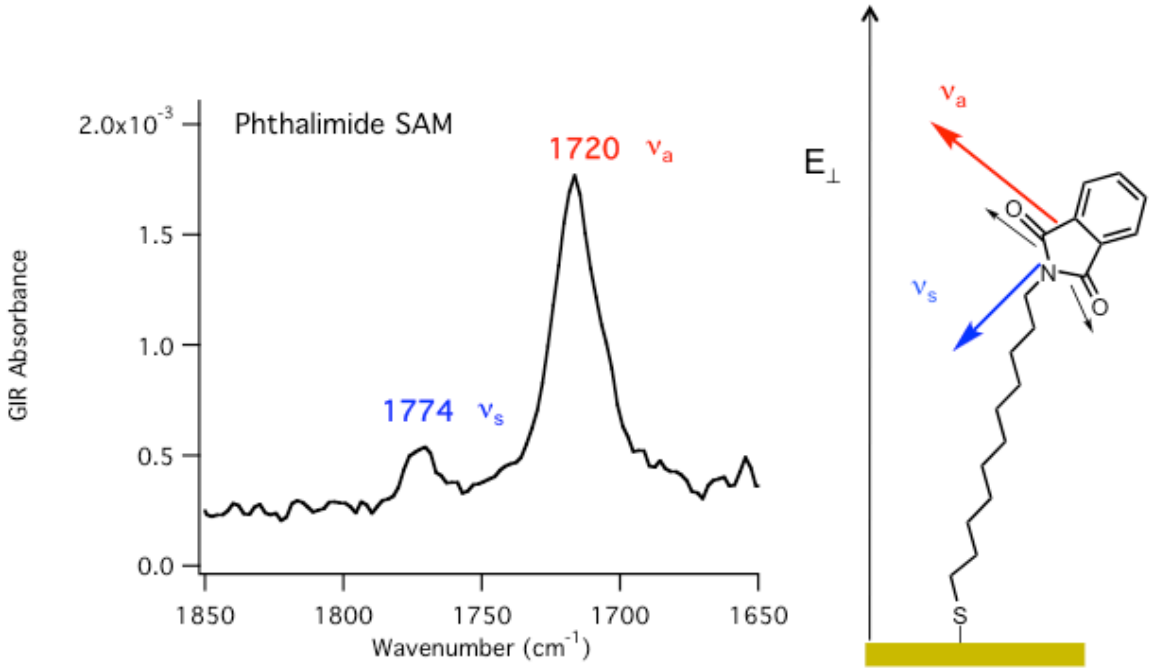

Figure 2-9. FTIR-GIR Spectrum of Molecule 1 adsorbed onto Gold substrate (SAM) and coupling with perpendicular electric field.

As the asymmetric dipole moment couples more strongly with the electric field perpendicular to the substrate, we observe ν_a to increase in intensity. In order to determine the magnitude of the increased absorbance intensity of ν_a(C=O), we compare it with the intensity at $\nu_a(CH_2)$ in the form of a ratio. Table 2-2 shows the absorbance intensity ratios for molecule **1** in different conformations (bulk, A, B, and C). The absorbance intensity ratio for molecule **1** in bulk is estimated to be 1.5 while that of Sample A is 1.3. We know that **1** in bulk is in crystalline form and in good order. The similarity in ratios between the two conformations suggests that molecule **1** is ordered in a similar manner when it is assembled into a monolayer (**A**). However, there is a distinguishable difference in the absorbance intensity ratio as **1** is spin-coated onto the gold surface to form Sample B. The increased ratio to 4.2 for Sample B suggests that the film is more ordered than the monolayer of **1**.

Table 2-2. Absorbance Intensities (a.u.) of Molecule 1 in different conformations

Sample	Asymmetric Phthalimide (C=O)	Asymmetric Methylene (CH_2)	Abs Intensity Ratio of ν_a(C=O) to $\nu_a(CH_2)$
Molecule **1** (bulk)	0.28	0.18	1.5
SAM of **1** (A)	0.0015	0.0011	1.3
Spincoated of **1** (B)	0.0038	0.00090	4.2
Annealed/Spincoated of **1** (C)	0.0012	No peak	N/A

The increased C=O intensity ratio to 4.2 in Sample **B** is attributed to the carbonyl group being oriented more perpendicular to the substrate and its dipole moment change is being maximized as it couples more strongly with the perpendicular electric field. Spincoating **1** molecules onto the gold surface for sample **B** may have forced the

attractive π-π interactions between the phthalimide groups to be stronger than the repulsive steric hindrance of the bulky terminal groups. However, keeping in mind that FTIR-GIR spectroscopy helps detect the entire monolayer and does not have the ability to isolate the air-monolayer interface, there is a possibility that this greater order does not have the advantage of exposing the phthalimide groups at the top of the film. There is a possibility that the alkyl chain of **1** has gauche kinks that may explain the weaker methylene peak signal compared to the stronger C=O coupling of the phthalimide group. By using immersion time as a variable in future experiments, we can investigate the possibility of gauche CH_2-CH_2 interactions and dispersion of bond angles and local environment as seen previously.[13]

2.3.2.3 Summary of FTIR-GIR Analysis

Molecule **1** is in crystalline, ordered form in bulk conformation while **1** conforms to a more disordered state in monolayer conformation. The monolayer is slightly more disordered than Samples B and C, suggesting that the packing density is poor. This is unexpected as we expected the isotropic (bulk) to be more disordered than the anisotropic self-assembled monolayer. However, as concluded by another study[12], the terminal groups at the air-monolayer interface can still be positioned at the top of the film and oriented perpendicular to the surface even if the alkyl chains may not pack in an orderly fashion. Low packing density does not necessarily reflect poorly on the photoreactivity of the phthalimide SAM because the other extreme of possessing high packing density can be problematic for making the phthalimide terminal groups less accessible.

2.3.3 XPS Spectra of pure Phthalimide-undecyl-thiol SAM and Thin films

X-ray Photoelectron Spectroscopy (Section 1.3.6) is used to characterize pure monolayer and thin films.[14] XPS is a characterization tool that we used to detect any changes in atomic composition between different conformations of **1**. In order to ascertain the correct assignment of fitted peaks for carbon 1s XP spectra of **1**, we have analyzed H-Phthalimide and N-Methyl Phthalimide as our model compounds.

2.3.3.1 XPS of model compounds

High-resolution spectra of phthalimide model compounds were compared with the phthalimide SAM (A), spincoated (B), and annealed/spincoated (C). H-phthalimide and N-methyl phthalimide hold the same core composition for the high-resolution carbon 1s spectrum of molecule **1** (Figure 2-10). As listed in Table 2-3, the fitted peaks as seen in the XP spectra are associated with three different chemical environments: C-C aliphatic/aromatic carbons, C-N carbons, and C=O carbons. While there are these similarities, the differences become more obvious when a methyl group or an undecyl hydrocarbon chain for N-methyl phthalimide and molecule 1 replaces the hydrogen atom in the H-phthalimide, respectively. The C=O peak, in particular, shifts to a greater binding energy as it becomes more difficult to abstract a core electron from the carbonyl carbon that lost electron density to the neighboring alkyl group. The fitted peak values compared with those found in literature[15] are similar to the experimental results.

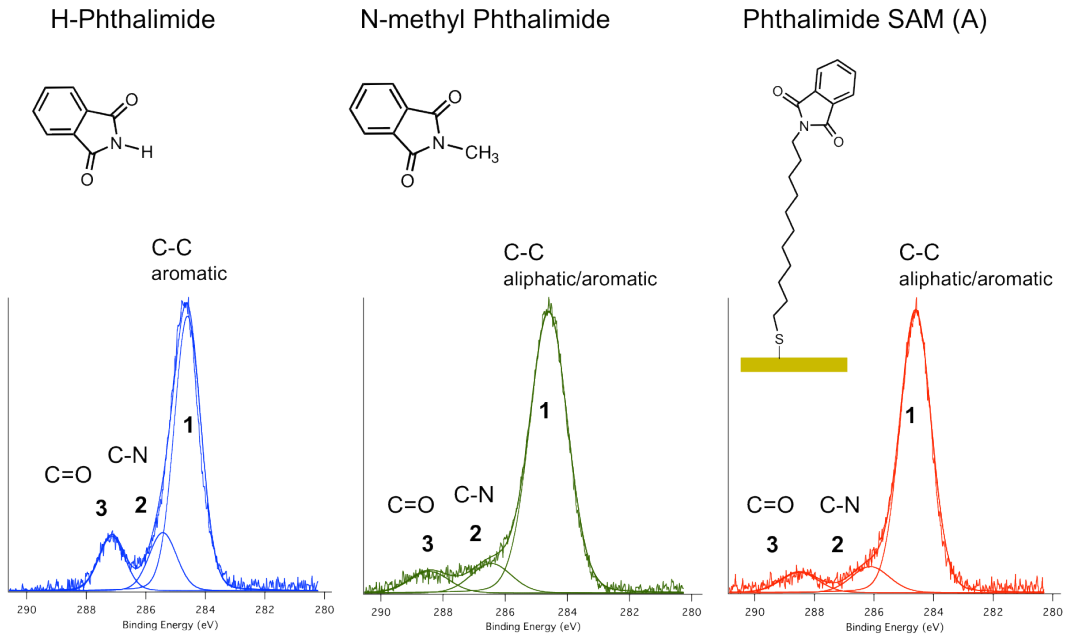

Figure 2-10. High-Resolution XP Spectra of C 1s of H-Phthalimide, N-Methyl Phthalimide, and SAM of Molecule 1 at take-off angle of 45 degrees.

Table 2-3. Fitted Peak Assignments of C 1s peak in XP spectra of Molecule 1 analog films and Monolayer at take-off angle of 45 degrees.

Sample	Fitted Peak #	Peak Energy (eV)	Peak Area %	Peak Assignment
(A) H-Phthalimide	1	284.6	70.9	C-C aromatic
	2	285.4	15.4	C-N
	3	287.1	13.7	C=O
(B) CH_3-Phthalimide	1	284.6	83.9	C-C aliphatic/aromatic
	2	286.4	9.4	C-N
	3	288.4	6.7	shifted C=O
(C) Monolayer of **1**	1	284.6	77.6	C-C aliphatic/aromatic
	2	286.1	10.9	C-N
	3	288.5	11.4	shifted C=O

For the monolayer of **1**, we expect the 14 aliphatic and aromatic carbons from the hydrocarbon chain and phthalimide's benzene group to contribute approximately 74%, three carbons surrounding the nitrogen to contribute 16%, and two carbonyl carbons in the phthalimide group to contribute 10%, out of a total of 19 carbons in the SAM molecule. We observe a close correlation with the experimental results shown in Table 2-3.

2.3.3.2 ADXPS Analysis of 1 in Monolayer and Films

Angular Dependent X-ray Photoelectron Spectroscopy (ADXPS) is known to be one of the useful techniques to investigate the molecular orientation of thin layer materials on solid substrates. This technique was used to investigate the orientation of dodecanethiol self-assembled monolayer on gold surface.[16].

XP spectra shown in Figure 2-11 provide quantitative information of **1** in Samples A, B, and C. The high-resolution C(1s) spectra show evidence of three different types of carbon. As indicated in Figure 2-11, the signal at 284.6 eV is associated with aliphatic and aromatic carbons that are not bonded to oxygen; the 286.1 eV signal is associated with C-N carbons and the carbons neighboring the carbonyl carbons in the phthalimide group; and the 288.3 eV signal is associated with phthalimide carbonyl carbon. Understanding that the depth of penetration is approximately 0.7 nm[17] at take-off angle of 15 degrees, XPS can be used to confirm that the phthalimide terminal groups of molecule **1** are situated at the top of the monolayer and oriented normal to the surface for Sample **A**.

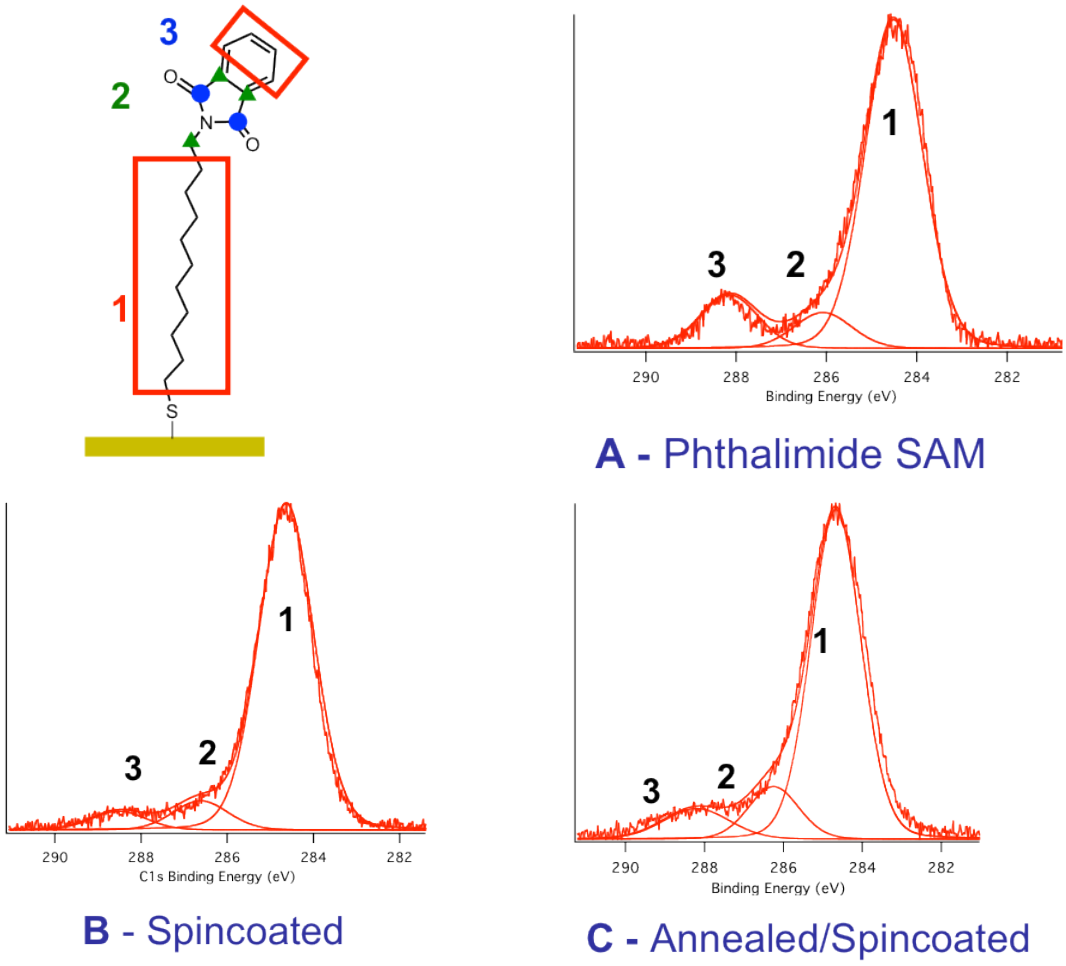

Figure 2-11. High-resolution XPS C(1s) spectra of Samples A, B, C collected with takeoff angle at 15 degrees.

Through the integrated peak intensities associated with each carbon environment, we notice that peak 3 (associated to the C=O) is more prominently displayed for sample A than for B or C. In Table 2-4, the intensity ratios for each sample are listed. We observe that peak 3 is not as strongly detected in Samples B and C, which is most likely due to a signal attenuation and relates back to how the samples were prepared. When **1** molecules were spin-coated onto the surfaces to produce samples B and C, the adsorbates were possibly "locked" into its resulting structure with the phthalimide terminal groups embedded inside the film rather than being exposed at the top. Sample C displayed the

highest peak 2:3 intensity ratio of 1.72 because the carbonyl peak was weakly detected at take-off angle of 15 degrees. This is a possible indication for a greater presence of hydrocarbon moieties closer to the surface. On the other hand, there was a stronger detection of the carbonyl group in Sample **A**, producing an intensity ratio of 0.96. The carbonyl signal is of interest in this study because it is the functional group responsible for photo-grafting.

Table 2-4. Intensity Ratios of Fitted Peaks 2 and 3 of XP C1s high resolution spectra of Samples A, B, and C

Sample	A	B	C
Intensity Ratio 2:3	0.96	1.56	1.72

Table 2-5 shows the atomic composition and the calculated C/Au ratio for all three samples. The C/Au ratio can be used as an indicator for the thickness and composition of the films. C/Au ratio is the lowest at 1.57 for Sample A, while it is highest at 6.9 for Sample C. The monolayer has a lower thickness value than the spincoated films (Samples B and C) and therefore, lower carbon content with respect to gold signal detected.

We also observe that there is higher oxygen content for samples B and C. Spin-coating molecule **1** onto surfaces in ambient conditions may have forced oxygen incorporation into the film composition. Notice how the oxygen atomic percentage increased from Sample A to B/C with the percentage increasing from 9.6% to at least 23% and 29%, respectively.

Table 2-5. Atomic Percentages for Phthalimide-thiol Samples Determined from Fitting XP Spectra collected at take-off angle (TOA) of 15°

Peak	A	B	C
Au 4f	23.89	8.2	9.2
C 1s	61.2	59.6	63.6
N 1s	5.4	3.0	4.15
O 1s	9.6	29.0	23.0
C/Au	1.57	4.28	6.9

2.3.3.3 Thickness Measurements: ADXPS, Molecular Model, Ellipsometry

The thickness values of A, B, and C may be estimated through angular dependent XPS (ADXPS) measurements by varying the photoelectron take-off angles – 45°, 35°, 25°, and 15°. In order to estimate the thickness of A, B, and C, the ratio of signals from the overlayer [C(1s)] and the substrate [Au($4f_{7/2}$)] was measured as a function of the takeoff angle. Based on Equation 2-1, the experimental data is fitted onto a linear regression plot as shown in Figure 2-12, and the overlayer thickness was derived from the slope of 0.0412. The slope was divided by 0.08, the overlayer coverage of 8% for coverage on gold substrates and then multiplied by the photoelectron mean free path of 2.25 nm to produce the thickness value of 1.16 nm. However, this value is then averaged with other trials and produced an average thickness value of 0.8 ± 0.3 nm for monolayer of **1** (Sample A).

Using the uniform overlayer model and assumption that the photoelectron mean free path is 2.25 nm[18], the thickness values were also calculated for Samples B and C to be 1.8 and 1.94 nm, respectively.

Equation 2-1: $\frac{I_L}{I_S} = \frac{Y_L}{Y_S}\left[\exp\frac{d}{\lambda\sin(\theta)} - 1\right]$

Y: yield (photoionization cross-section)
I_L: Signal from overlayer (C 1s)
I_S: Signal from substrate (Au 4f)
D: thickness of overlayer
λ: Photoelectron mean free path
θ: take-off angle

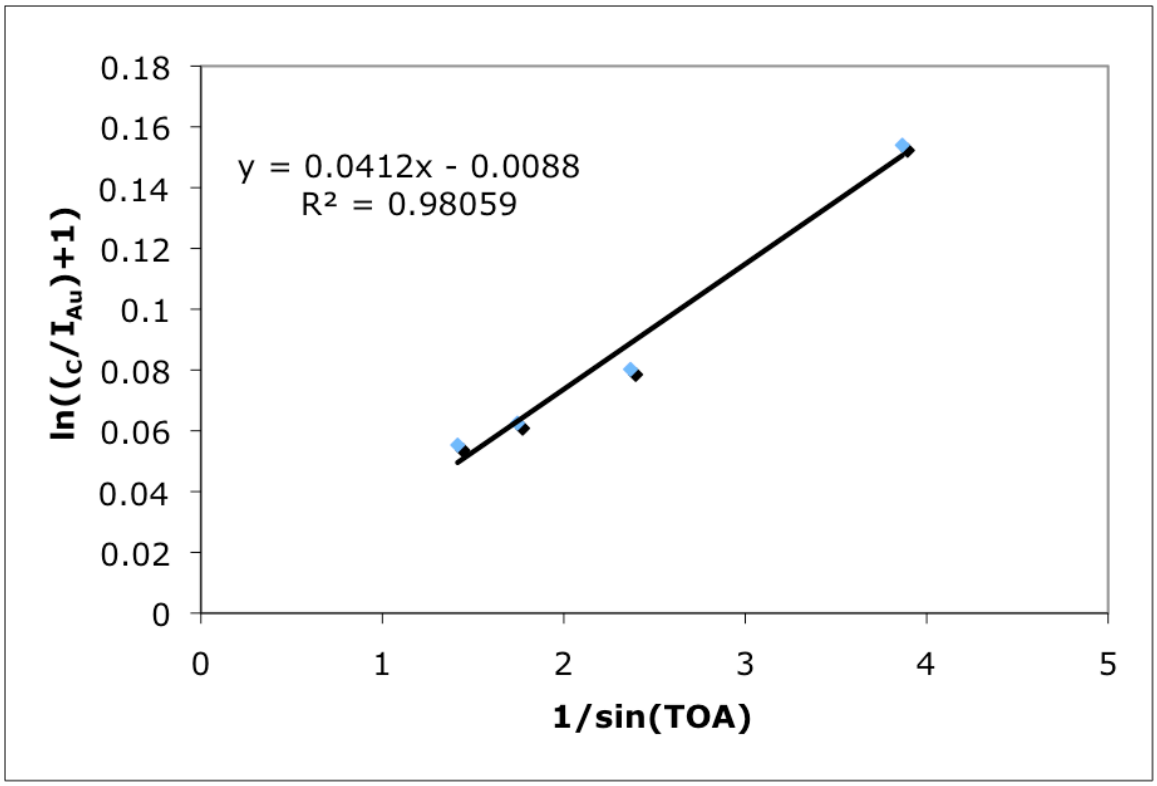

Figure 2-12. Substrate-Overlayer Model of SAM of Molecule 1 to show how the thickness value was calculated from XP spectra collected at take-off angles of 45, 35, 25, and 15 degrees.

Table 2-6 provides a summary of thickness values calculated from the molecular model (Spartan) to ADXPS and ellipsometry.

Table 2-6. Estimated Thickness values

SAMPLE	A	B	C
Molecular Model (nm)	2.19	N/A	N/A
ADXPS Estimated Thickness (nm)	0.8 ± 0.3	1.8 ± 0.3	1.94
Ellipsometric Thickness (nm)	1.38	1.58	1.18

Spartan Pro molecular modeling program was used to calculate the minimized energy of the structure for molecule **1**, as drawn in Figure 2-13. The bond angles and lengths were measured on the structure with minimized energy and used to find the total molecular length of 2.19 nm.

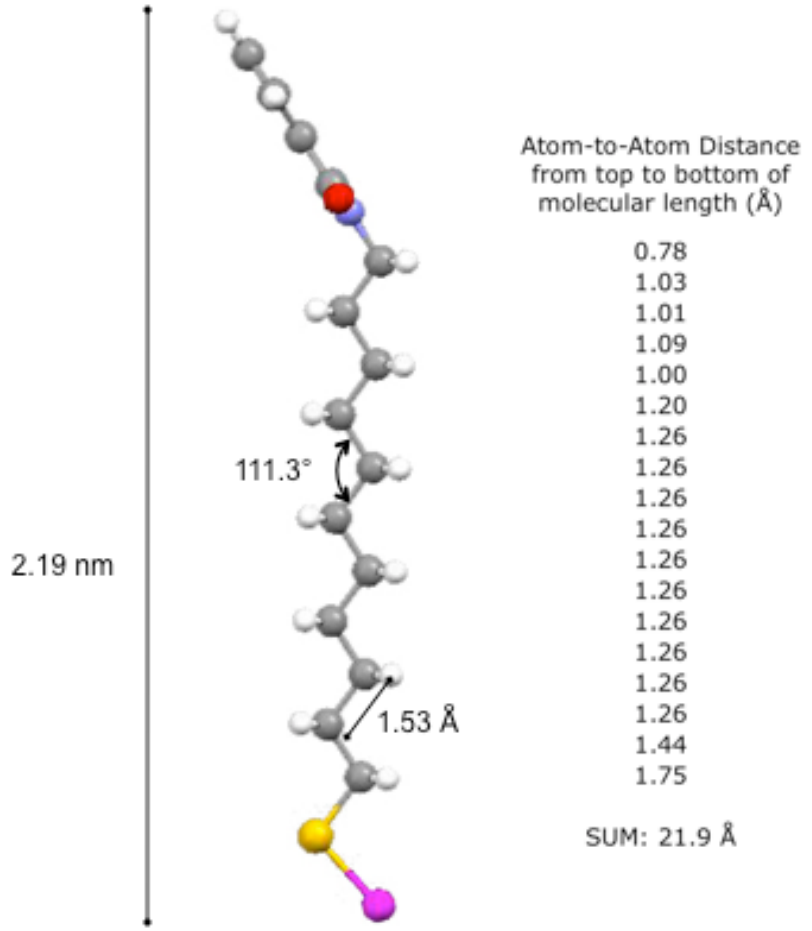

Figure 2-13. Minimized Energy Structure of Molecule 1.

From the molecular model of **1** and the experimental thickness values, we calculated an *average* tilt angle of the molecule in the monolayer (Sample A). With the ADXPS estimated thickness average of 0.8 nm, the tilt angle was averaged to be 68.7 degrees. With the ellipsometric thickness, the tilt angle was calculated to be 50 degrees. The tilt angle calculation is an approximation because we cannot guarantee that every adsorbate on the surface will oriented at that particular angle. There will be patches in the overlayer with different α, β, and χ.

2.4 Summary and Outlook

The focus of this chapter was on the self-assembled monolayer of molecule **1** and its overall structure and composition. In order to achieve a detailed understanding of Sample A, other similar systems were also analyzed for comparison. FTIR-GIR Spectroscopy, ADXPS, and Ellipsometry together produced a comprehensive picture of the orientation of **1** with respect to the surface of a gold substrate.

FTIR-GIR results demonstrated that the self-assembled monolayer (Sample A) was not as ordered as the other systems (Sample B and C). A more disordered film suggests that the packing density and coverage are low. Low surface coverage is not necessarily a disadvantage for the phthalimide-undecyl-thiol monolayer because high packing density is known to decrease the photo-reactivity of the phthalimide terminal group. One possible explanation for the Samples B and C to be more ordered is that spin-coating applied a force that overcame any steric hindrance between the adsorbates and packed the molecules closely together.

High-resolution XP spectra of C 1s for samples A, B, and C show three characteristic peaks for phthalimide-undecyl-thiol, as confirmed by the model compounds used to vary the peak positions. With ADXPS, we were able to closely analyze each film at a take-off angle of 15 degrees and illustrate that Sample A was different from the other two samples. Monolayer of **1** displayed a more pronounced peak 3 (associated to phthalimide carbonyl) at take-off angle of 15 degrees and limited depth of penetration of 0.7 nm. The shallow depth of penetration produces XPS results that pertain to only the top part of the monolayer or film and offers more information about the orientation of molecule **1** on the surface. Samples B and C produced an attenuated C=O signal while

Sample A (monolayer of less than 1 nm thin) produced a pronounced C=O peak at the air-monolayer interface. Understanding the structure of phthalimide SAM plays an important role in improving its photo-grafting abilities.

For further analysis of the self-assembly process of molecule **1**, Scanning Tunneling Microscopy can be used to look more closely at the different phases – lying down vs. standing up conformation. In addition, FTIR-GIR spectroscopy can be used to monitor photo-reactivity of phthalimide SAM real-time and study more improved monolayer systems (mixed SAMs).

2.4.1 Outlook: Exploring Photoreactivity of Phthalimide SAM

Further experiments would be to study the photo-reactivity of phthalimide SAM by quantifying the changes in the C=O region in FTIR-GIR spectrum upon UV exposure and grafting of another species onto the surface. Upon photoreaction of the phthalimide group with the assumption that both carbonyls will not be photoreduced, the initial carbonyl peak is expected to decrease in absorbance intensity. Another expected change is a carbonyl peak shift to higher wavenumber due to less conjugation with the benzene and other imide carbonyl.

2.4.2 Outlook: Mixed Phthalimide SAMs

As discussed in Section 2.1.1, mixed self-assembled monolayers have the potential to improve surface coverage and any surface chemistry that follows. When another molecule is introduced to a pure self-assembled monolayer of **1**, there is a greater likelihood that the mixed SAM will have greater order and surface coverage, which may improve the phthalimide's photo-grafting capabilities.

2.5 Acknowledgements

We would like to thank our collaborators, Professor John Rabolt and Bruce Chase, at University of Delaware and PA-IR Technologies, LLC.

2.6 References

1. (a) Ulman, A., Formation and Structure of Self-Assembled Monolayers. *Chem. Rev.* **1996,** *96*, 1533-1554; (b) Rehak, M.; Snejdarkova, M.; Otto, M., Application of biotin-streptavidin technology in developing a xanthine biosensor based on a self-assembled phospholipid membrane. *Biosens. Bioelectron.* **1994,** *9*, 337-341; (c) Delamarche, E.; Sundarababu, G.; Biebuyck, H.; Michel, B.; Gerber, C.; Sigrist, H.; Wolf, H.; Ringsdorf, H.; Xanthopoulos, N.; Mathieu, H. J., Immobilization of Antibodies on a Photoactive Self-Assembled Monolayer on Gold. *Langmuir* **1996,** *12*, 1997-2006.

2. (a) Poirier, G. E., Coverage-dependent phase and phase stability of decanethiol on Au(111). *Langmuir* **1999,** *15*, 1167-1175; (b) Godin, M.; Williams, P. J.; Tabard-Cossa, V.; Laroche, O.; Beaulieu, L. Y.; Lennox, R. B.; Grutter, P., Surface Stress, Kinetics, and Structure of Alkanethiol Self-Assembled Monolayers. *Langmuir* **2004,** *20*, 7090-7096.

3. Bensebaa, F.; Voicu, R.; Huron, L.; Ellis, T. H., Kinetics of Formation of Long-Chain n-Alkanethiolate Monolayers on Polycrystalline Gold. *Langmuir* **1997,** *13*, 5335-5340.

4. Calvente, J. J.; Lopez-Perez, G.; Jurado, J. M.; Andreu, R.; Molero, M.; Roldan, E., Reorientation of Thiols during 2D Self-Assembly: Interplay between Steric and Energetic Factors. *Langmuir* **2010,** *26*, 2914-2923.

5. Vericat, C.; Vela, M. E.; Benitez, G.; Carro, P.; Salvarezza, R. C., Self-assembled monolayers of thiols and dithiols on gold: new challneges for a well-known system. *Chem. Soc. Rev.* **2010,** *39*, 1805-1834.

6. Heid, S.; Effenberger, F.; Bierbaum, K.; Grunze, M., Self-Assembled Mono- and Multilayers of Terminally Functionalized Organosilyl Compounds on Silicon Substrates. *Langmuir* **1996** *12*, 2118-2120.

7. Love, J. C.; Estroff, L. A.; Kriebel, J. K.; Nuzzo, R. G.; Whitesides, G. M., Self-Assembled Monolayers of Thiolates on Metals as a Form of Nanotechnology. *Chem. Rev.* **2005,** *105*, 1103-1169.

8. Kwon, Y.; Mrksich, M., Dependence of the Rate of an Interfacial Diels-Alder Reaction on the Steric Environment of the Immobilized Dienophile: An Example of Enthalpy-Entropy Compensation. *J. Am. Chem. Soc.* **2002,** *124*, 806-812.

9. Bieniarz, C.; Cornwell, M. J., A Facile, High-Yielding Method for the Conversion of Halides to Mercaptans. *Tetrahedron Letters* **1993,** *34*, 939-942.

10. Rabolt, J. F.; Burns, F. C.; Schlotter, N. E.; Swalen, J. D., Anisotropic orientation in molecular monolayers by infrared spectroscopy. *J. Chem. Phys.* **1983,** *78*, 946-952.

11. Rigout, M. L. A.; Lewis, D. M., Use of Fourier Transform Infrared Spectroscopy to Follow the Heterocumulene Aided Thermal Dehydration of Phthalic and Napthalic Acids. *Applied Spectroscopy* **2006,** *60*, 1405-1413.

12. Yang, D. B.; Wakamatsu, T., Polarized Grazing Angle FTIR Study of Molecular Orientation and Bonding of Thioglycolates at the Metal Interface. *Surface and Interface Analysis* **1996,** *24*, 803-810.

13. Terrill, R. H.; Tanzer, T. A.; Bohn, P. W., Structural Evolution of Hexadecanethiol Monolayers on Gold During Assembly: Substrate and Concentration Dependence of Monolayer Structure and Crystallinity. *Langmuir* **1998,** *14*, 845-854.

14. (a) Brundle, C. R.; Carley, A. F., Electron Spectroscopy and Adsorption Studies: Chemical Shifts in X-ray Photoelectron and Auger Spectra for Monolayer Adsorption. *Chemical Physics Letters* **1975,** *33*, 41-45; (b) Merzlikin, S. V.; Tolkachev, N. N.; Strunskus, T.; Witte, G.; Glogowski, T.; Woll, C.; Grunert, W., Resolving the depth coordinate in photoelectron spectroscopy - Comparison of excitation energy variation vs.

angular-resolved XPS for the analysis of a self-assembled monolayer model system. *Surface Science* **2008,** *602*, 755-767.

15. Chenite, A.; Selmani, A., Cr/phthalimide system: XPS study of interfacial reactions. *Surface Science* **1994,** *301*, 197-202.

16. Kondo, T.; Yanagida, M.; Shimazu, K.; Uosaki, K., Determination of Thickness of a Self-Assembled Monolayer of Dodecanethiol on Au(111) by Angle-Resolved X-ray Photoelectron Spectroscopy. *Langmuir* **1998,** *14*, 5656-5658.

17. Fadley, C. S.; Baird, R. J.; Siekhaus, W.; Novakov, T.; Bergstrom, S. A. L., Surface analysis and angular distributions in x-ray photoelectron spectroscopy. *Journal of Electron Spectroscopy and Related Phenomena* **1974,** *4*, 93-137.

18. Fadley, C. S., Solid State and Surface Analysis By means of Angular-Dependent X-ray Photoelectron Spectroscopy. *Progress in Solid State Chemistry* **1976,** *11*, 265-343.

3 Application of Phthalimide SAM to Produce NP-Films

3.1 Introduction: Nanotechnology and Surfaces

The fabrication of nanoparticle (NP)-films on surfaces holds potential applications in optical, electronic, and biological systems due to the NPs' distinct advantage in small size and high surface area to volume ratio.[1] Enthusiasm for nanotechnology predominantly originates from the unique size-dependent property of nanoparticles (NP). However, individual NPs cannot deliver the expected performance in actual devices and commercial applications because only a large number of NPs in robust assemblies can display such a quality. Therefore, research efforts have been made to develop NP-assembly methods with controlled spatial distribution and geometry. Currently, manipulating NPs on a large scale is a great challenge. By tethering NPs to surfaces, we are able to increase surface functionality.[2] Nanoparticle-films can be patterned with conventional photolithographic methods and fabricated by a range of techniques: dip and spincoating[3], layer-by-layer assembly[4], and spray coating[5] from supercritical fluids or water. The efficacy of the technique is demonstrated in the wear resistance and strength of the NP-films fabricated.

NP-grafting has been done previously using a variety of chemical reactions[6], but only photo-grafting technique is known[2], where microemulsions were surface tethered via photoinitiation of the benzophenone functional group. Other NP-film fabrication techniques include lithography.[7] However, these methods particularly lithographic techniques are costly, have limitations in its approach and produce unstable, non-covalent surface attachments of the NPs to the surface.

In response to the demands to develop a technique that is simple and inexpensive, it is highly desirable to design a photochemical method. Photo-grafting is potentially a "universal technique" that would tether essentially any organic NP to a surface. We show that a photo-functionalized monolayer composed of phthalimide groups provides an example that possesses the desirable properties of such a universal method. Previously we have shown that this simple photochemical approach that has been used to graft polymers of small to high molecular weight, particularly carbohydrates, to glass and silicon surfaces in order to build biodiagnostic microarrays.[9]

In collaboration with Professor Robert Prud'homme from Princeton University, we have the ability to anchor drug delivery nanosphere to material surfaces by using this photochemical method. We extend the photografting technique to fabricate well-controlled NP-films, using polymeric nanoparticles (PNPs), composed of a polystyrene (PS)-Hostasol red dye core and a polyethylene glycol (PEG) shell. In Figure 3-1, the PNPs are schematically shown to be immobilized onto the surface via the photoinduced phthalimide self-assembled monolayer. At the air-monolayer interface in the light-exposed regions where the photochemistry occurs, a covalent bond causes the PNPs to adhere to the glass or silicon substrate. Here, the PNPs were intentionally drawn as "flattened" spheres and will be discussed later in this chapter.

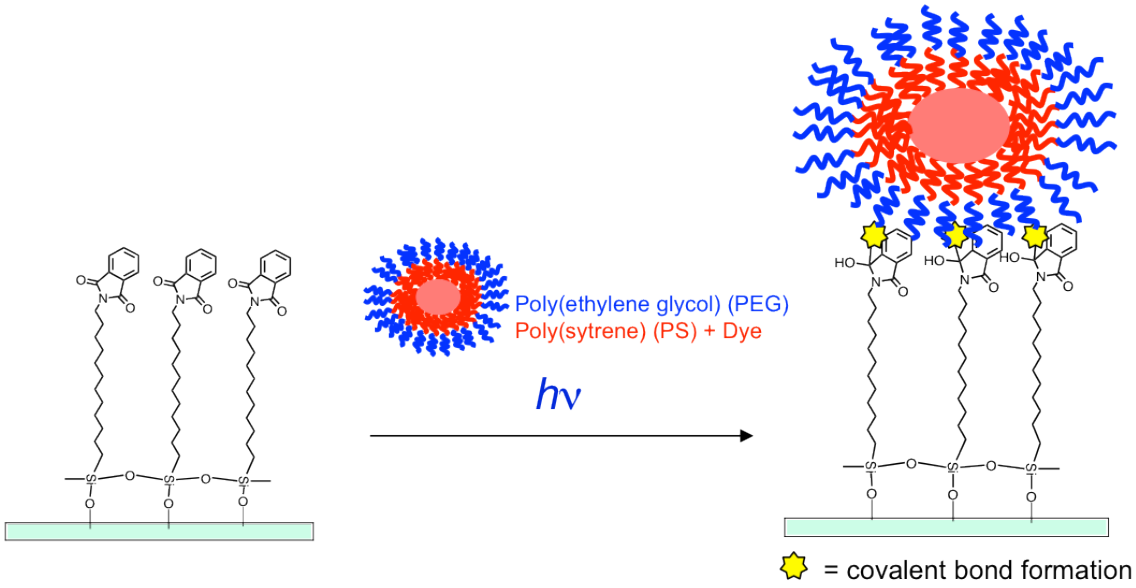

Figure 3-1. Schematic illustration of grafting PNPs to the photofunctionalized surface (glass or silicon). Figure is not drawn to scale.

3.2 Methods

3.2.1 Synthesis of Alkyne-decorated Polymeric Particles.[10]

Fluorescent nanoparticles were assembled via Flash NanoPrecipitation[11] using polystyrene (PS)-poly ethylene oxide (PEO) diblock copolymers. Hostasol red, a hydrophobic fluorescent dye, was encapsulated inside the core of the polymeric nanoparticles. To generate nanoparticles with 20% surface alkyne coverage, hydroxyl terminated block copolymer PS-*b*-PEO-OH (8 mg/mL, 1.8 mM, PS Mw ~ 1500, PEO Mw ~ 3000), alkyne terminated block copolymer PS-*b*-PEO-alkyne (2 mg/mL, 0.44 mM, PS Mw ~1500, PEO Mw~3000), homopolymer PS-OH (10 mg/mL, 6.7 mM, Mw~1500), and hostasol red (0.01 mg/mL, 30 μM) were dissolved in THF, a water-miscible organic solvent (12 mL/min), and rapidly mixed with three water streams (each at 40 mL/min). Immediately after the nanoparticle assembly, THF was removed by dialysis against

ultrapure water using Spectra/Por dialysis tubing with a molecular weight cutoff of 6000-8000.

The surface coverage of these polymeric particles can be easily adjusted by changing the ratio between -OH terminated polymer and -alkyne terminated polymer. The particles used for this particular study had approximately a 20% alkyne coverage. The free alkyne groups can be used for further biological click chemistry (alkyne-azide cycloaddition) applications to graft azide-functionalized biomolecules such as DNA onto the particle-modified surfaces.[10c, 12] From dynamic light scattering, it was determined that these polymeric NPs are approximately 100 nm in diameter in aqueous solution.

3.2.2 Synthesis of phthalimide-undecyl-trimethoxysilane[9]

A 3.3 mmol portion of 11- bromoundecanetrimethoxysilane (Gelest) was added to a solution of an equimolar amount of potassium phthalimide (Aldrich) in 60 mL of anhydrous dimethylformamide (DMF; Aldrich). The solution was stirred overnight at room temperature (RT) under argon. Chloroform (50 mL) was added. The solution was transferred to a separatory flask containing 50 mL of H_2O. The aqueous layer was separated and then extracted with two 20 mL portions of chloroform. The combined chloroform extract was washed with several 20 mL portions of H_2O. The chloroform was removed by rotoevaporation, and residual DMF was removed on a high vacuum line to give a pale yellow oil.

3.2.3 Self-Assembly of Phthalimide-undecyl-trimethoxysilane onto Glass or Silicon wafer

The solid substrates consisted of glass (ArrayIt) or silicon (Wafer world) typically with dimensions of 2.54 cm × 7.62 cm, but for XPS sample dimensions were smaller (1

cm × 1 cm). The substrates and glassware were cleaned in piranha solution (2:1 H_2SO_4: 30% H_2O_2) for 2 hours followed by extensive rinse with water and ethanol. Substrates were dried with a stream of argon and immersed in a 1 mmol solution of phthalimide-undecyl-trimethoxysilane in anhydrous toluene (Aldrich). Substrates were kept in solution for 12 h in dark. The resulting SAMs were rinsed with toluene and sonicated three times for 2 min each in toluene, toluene/methanol (1:1), and methanol. Substrates were kept in argon-purged containers until further use.

3.2.4 Photochemical Grafting and Patterning of Polymeric NP-Films

Polymeric NPs (PNPs) in aqueous solution were spin-coated onto phthalimide SAM-functionalized glass or silicon substrates at 3000 rpm for 1 min and placed in argon-purged containers. Spin-coated surfaces were irradiated at 254 nm for 15 min with a Rayonet photochemical reactor. Samples were rinsed with water, dried with argon, and immediately analyzed by techniques described below.

To pattern a PNP-film, a 400-mesh transmission electron microscopy (TEM) grid (Electron Microscopy Sciences) was used as a photomask for all patterning experiments. After spin-coating PNPs onto phthalimide SAM-functionalized substrate, the photomask was placed on top of the PNP-coated substrate. Irradiation was carried out with a desktop lamp containing a 254 nm Rayonet bulb for approximately 15 min. The photomask was removed and photopatterned surface was rinsed with water and blown dry with argon, prepared for analysis.

For both cases (with or without pattern), two sample groups were prepared: (1) Irradiated surfaces as described above and (2) Non-irradiated surfaces. The non-irradiated samples were prepared as follows. As the non-irradiated surfaces serve as

'dark' control samples, the phthalimide-functionalized SAMs were treated as close as possible to the irradiated samples except the irradiation step was eliminated. For non-irradiated samples, the PNPs were spin-coated onto the SAM-substrate, *not* exposed to light, rinsed with water, blown dry with argon, and prepared for technical analysis. The dark controls can indicate whether or not PNPs are adhering to the surface via physisorption or chemisorption. We expect the dark controls to demonstrate that PNPs cannot strongly bind to surfaces in the absence of light.

3.2.5 Spectroscopic Characterization Methods

Contact Angle Goniometry. Static contact angle measurements were performed with a Rame-Hart 100-00 contact angle goniometer using Millipore Mili-Q water. With the use of a micropipet, a drop of 6-μL volume was placed directly onto the sample. At least three droplets were measured on each sample.

X-ray photoelectron spectroscopy (XPS) spectra were recorded with a PHI 5500 spectrometer equipped with a hemispherical electron energy analyzer, a multichannel detector, and an Al Kα monochromator X-ray source run at 15 kV and 23.3 mA. The test chamber pressure was maintained below 2×10^{-9} Torr during spectral acquisition. A low-energy electron flood gun was used as required to neutralize surface charging. The binding energy (BE) was internally referenced to the aliphatic C 1s peak at 284.6 eV. Survey spectra were acquired using an analyzer pass energy of 93.9 eV and a BE resolution of 0.8 eV, while high-resolution spectra were acquired with a pass energy of 23.5 eV and a BE resolution of 0.05 eV. The takeoff angle is defined as the angle between the surface and the photoelectron detector. Spectra were deconvoluted using RBD software that fits a series of Gaussian-Lorentzian functions to each chemically

shifted photoelectron peak, after subtracting an appropriate background. Atomic concentrations were calculated by normalizing peak areas with the elemental sensitivity factor data in the PHI database. Note: The XPS samples were prepared with smaller dimensions (1cm × 1cm) and consequently, the spin-coating conditions were adjusted to 250 rpm for 1 min.

Atomic Force Microscopy (AFM) images were obtained with a ThermoProbes Autoscope CP Research System. Surfaces were imaged in non-tapping mode across 5.0 × 5.0 μm dimensions for the phthalimide SAM and 10.0 × 10.0 μm dimensions for the PNP-film.

Confocal Fluorescence Microscopy (CFM). The samples were analyzed using an inverted microscope with an Olympus Fluoview confocal system (New York/New Jersey Scientific, Middlebush, NJ) with dual wavelengths excitation at 488 and 568 nm (20× objective lens). Images were captured with 488 nm excitation wavelength.

3.3 Results and Discussion

The process of photo-grafting PNPs is illustrated schematically in Figure 3-1. The NP photo-grafting technique is based on a widely known photochemical mechanism that uses self-assembled monolayers (SAMs) containing aromatic carbonyls that react with C–H groups to form a covalent bond.[13] Benzophenone (BP) derivatives are among the most commonly used photoactive groups to develop biological membranes.[14] Similarly, phthalimide derivatives can undergo the same photochemical reaction to cause grafting of organic polymers whose mechanism can be described as follows (Figure 3-2). Upon absorption of a photon, the phthalimide group is excited to the n-π^* state; the latter electronically excited state abstracts a C-H hydrogen atom from a nearby molecule, in

this case a PNP, to form a radical pair, with one radical center firmly attached to the surface via the phthalimide group and the other firmly attached to the PNP. When the resulting radical pair recombines, a strong covalent bond is formed between the surface and the PNP. This covalent bond immobilizes the PNPs onto surfaces. It should be pointed out that other secondary processes such as disproportionation and back-transfer, that do not lead to grafting are also possible. However, although the grafting efficiency to these phthalimide-functionalized surfaces is quantitatively unknown, in practice, the photoactive monolayers have proven to be successful in fabricating carbohydrate microarrays with high signal throughputs.[9] The photoactive property of phthalimide-silane monolayer is the novel component of our NP-film fabrication technique and we show below that the concept works for the photografting of PNPs on to surfaces also.

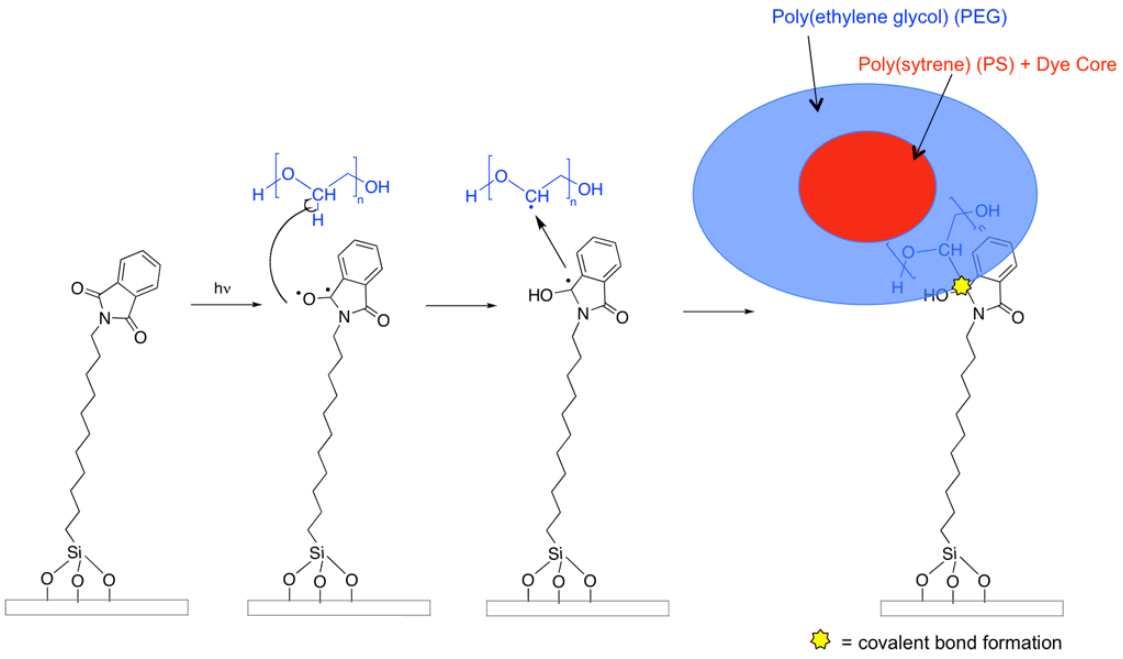

Figure 3-2. Phthalimide SAM photo-grafting PNPs via a hydrogen abstraction mechanism upon UV exposure. The phthalimide functional group undergoes a photochemical reaction where the excited carbonyl abstracts a hydrogen atom from the PEG polymer part of the nanoparticles, resulting in covalent bond formation from a radical-radical combination.

Standard surface techniques such as contact angle goniometry and ellipsometry were used for characterization of the pre-irradiated and irradiated films. Contact angle goniometric analysis of phthalimide SAM, prior to PNP-film application, produced a water contact angle of approximately 65 ± 1° as cited before in literature for this SAM.[9] However, upon photografting PNPs onto the SAMs, the contact angle results showed inconsistency in the left and right readings of each water droplet, which indicated film roughness. Similarly, ellipsometry could not be used to measure the thickness of the PNP-films due to difficulty in calculating the varying refractive indices between PNP-film and underlying phthalimide monolayer.

However, the photo-grafted PNP-films could be characterized by X-ray Photoelectron Spectroscopy (XPS), Atomic Force Microscopy (AFM) and Confocal Fluorescence Microscopy (CFM). Each of these techniques is powerful in some regards, but also possesses some limitations.

3.3.1 X-ray Photoelectron Spectroscopy (XPS) Results

XPS is a conventional surface characterization tool that we used to illustrate the differences in atomic composition between the samples before and after NP-grafting. XP spectra of the phthalimide SAM-functionalized glass substrates, before and after photo-grafting of the PNPs are shown in Figure 3-3 (a) and (b), respectively. Peaks are assigned to Si 2p (103.5 eV), Si 2s (155.0 eV), C 1s (284.6 eV), and O 1s (532.0 eV).[15] These peaks correspond to the atoms on the glass substrate, C bound to other carbons, hydrogens, and oxygens, and oxygen in silicon dioxide of the substrate.[15] One significant difference seen between the two spectra in Figure 3-3 is in the relative peak heights,

focusing on the increase of C1s signal and decrease of Si2p signal with the addition of the PNPs.

In order to quantify the magnitude of this change upon the PNP-film fabrication, the C1s and Si2p peaks were fitted and the percent atomic concentrations were quantified as shown in Table 3-1. This change is most noticeable in comparing the C/Si ratios for the two samples in the bottom line of Table 3-1. The increase of C/Si ratio from 1.46 (phthalimide SAM) to 5.67 (PNP-Film) is significant, in contrast to negligible change between the phthalimide SAM and dark control. The quantitative analysis of the peak area change indicates the PNPs were covalently bound to the glass substrates.

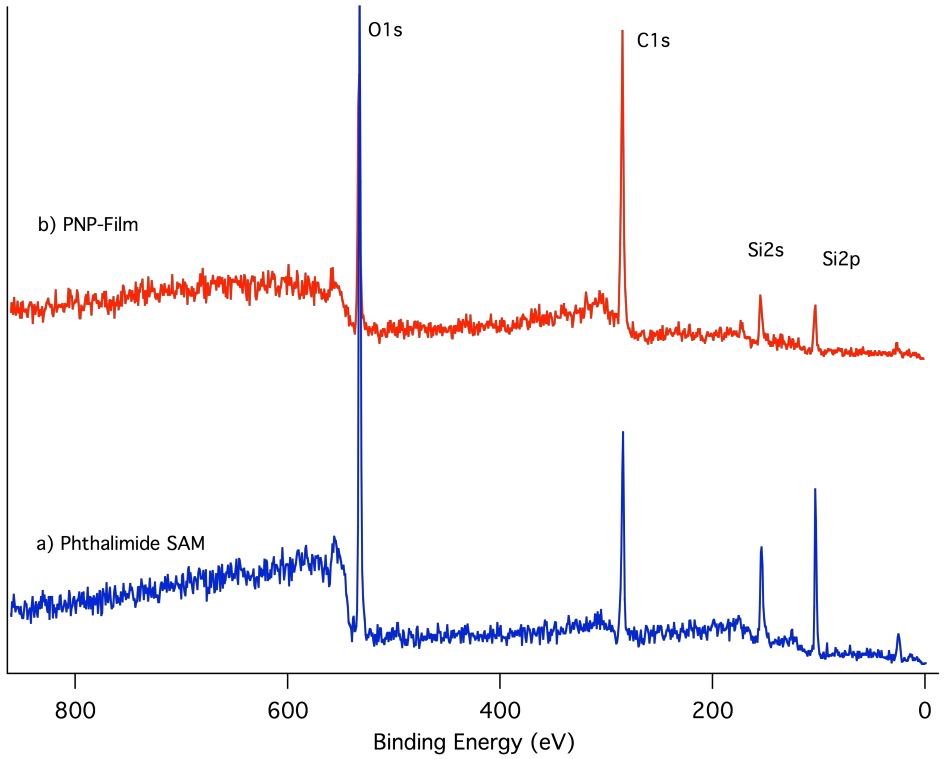

Figure 3-3. Survey Spectra of (a) Phthalimide SAM and (b) PNP-film deposited onto clean glass substrates at a take-off angle of 45 degrees.

Table 3-1. Atomic Percentages of Phthalimide SAM and NP-Film Determined from Fitting of XP Spectra

Peak	Phthalimide SAM	Dark Control	PNP-Film
C 1s	33.2	34.7	61.8
Si 2p3	22.7	20.1	10.9
C/Si	1.46	1.73	5.67

Furthermore, fitting of the high-resolution C1s spectra helps identify different chemical environments for the elements observed in XPS. The C1s peak for phthalimide SAM is well fit by three carbon components at 284.6, 286.1, and 288.0 eV, which can be attributed to C-C, C-N, and C=O carbons, respectively (Figure 3-4a). However, the PNP-film sample is fit by four carbon components at 284.6, 285.6, 287.2, and 291.9 eV (Figure 3-4b).

Figure 3-4b shows the disappearance of carbonyl peak at 288.0 eV indicative of the phthalimide SAM signal being overshadowed by PNPs and the appearance of a new peaks labeled 2-4, that can be attributed to the ether carbons from the PEG shell and π to π^* satellite structure from the PS core.

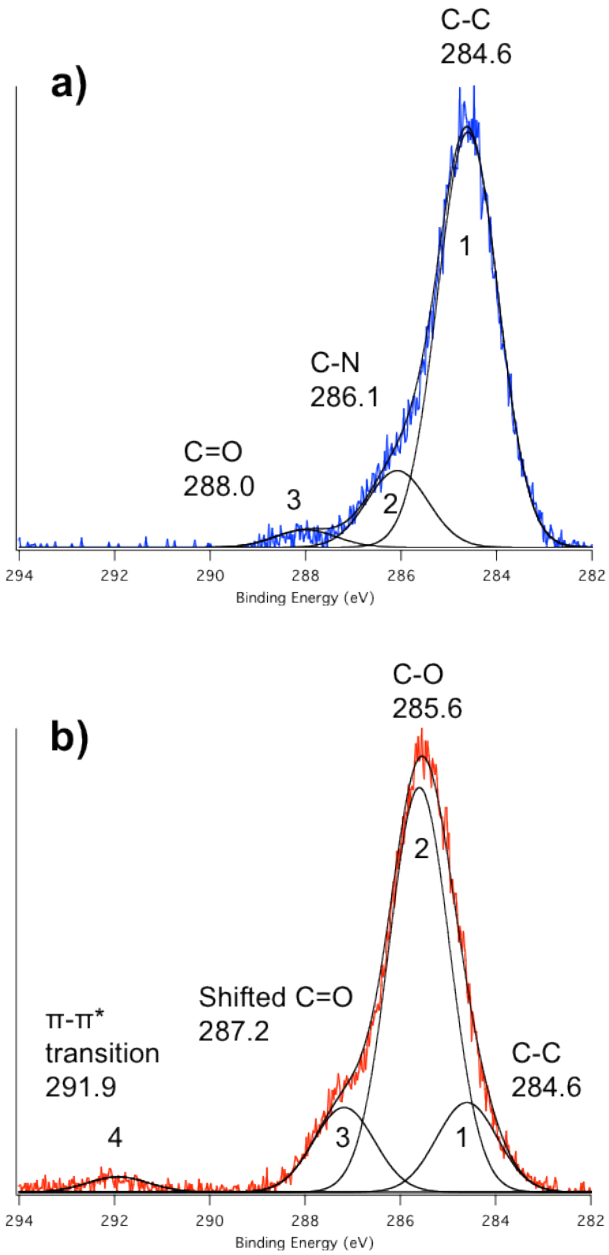

Figure 3-4. Fitted high-resolution corrected XP spectra of C 1s peak at 284.6 eV: (a) Phthalimide SAM and (b) Photo-grafted PNP-film on glass. XP spectra were collected with a take-off angle of 45 degrees. (20% alkyne terminated PEG-PS-Hred polymeric particles photografted onto phthalimide functionalized glass substrate.)

Looking more closely at the percentage peak areas in Table 3-2, we observe that the shake-up intensity of the PNP-film at 291.9 eV was estimated to be 2.5% of the C1s peak, while a typical shake-up intensity for pure polystyrene is 5-10%.[16] The weaker percentage of 2.5% for the PS π to π^* transition confirms the expected stronger signal from the PEG outershell and heterogeneous nature of the block copolymer NPs. The 'shake-up' process of the PS may appear different here in the PNP-film because the PS is integrated into a polymeric nanoparticle core and therefore, may have a different glass transition temperature T_g compared to pure PS. In addition to the different chemical environment being surrounded by PEG, the lower molecular weight of the PS core can contribute to the lower shake-up intensity.

The peak area percentage values of the samples before and after photo-grafting provide more quantitative information to indicate the presence of PNPs that were photo-grafted to the surface (shown in Table 3-2). Before PNP-grafting, the phthalimide SAM is closely analyzed by comparing the experimental peak area % values with the estimated/expected values. For phthalimide SAM, we expect the 14 aliphatic and aromatic carbons from the hydrocarbon chain and phthalimide's benzene group to contribute to approximately 74%, three carbons surrounding the nitrogen to contribute 16%, and two carbonyl carbons in the phthalimide group to contribute 10%, out of a total of 19 carbons in the SAM molecule. The peak area percentages (experimental and expected values) are closely related enough to identify characteristic peaks of the phthalimide SAM on the surface.

For the photo-grafted PNP-film, we notice that the peak area percentage values change significantly as new carbon environments are introduced and additional fitted

peaks appear. We have already discussed the characteristic peak of polystyrene's π to π* transition. The formation of fitted peak at 285.6 eV represents one of the two most significant changes upon PNP-grafting with the ether carbons making up 68% of the total carbon environment. The sharp increase in intensity of the ether carbon peak was expected as our spectral results were compared to the standard XP spectrum of a PEG polymer film.[17] The other large difference was observed in the aliphatic carbon peak at 284.6 eV as its peak area dropped to 15% of the total. With the same take-off angle at 45 degrees, the x-ray beam penetrates the same distance into the PNP-film as it did the phthalimide SAM. Given the same depth of penetration, the XP spectral results more strictly correspond to the grafted polymeric nanoparticles, as opposed to the SAM itself. This explains the largest peak area of 68% relating to the PEG component of the PNPs.

Table 3-2. Fitted Peak Assignments of C 1s peak in XP spectra of Phthalimide SAM and photo-grafted PNP-film. Take-off angle of 45 degrees.

Sample	Element/ Transition	Peak Energy (eV)	Peak Area %	Peak Assignment
(A) Phthalimide SAM	C 1s	284.6	81.5	C-C aliphatic
	C 1s	286.1	15.0	C-N
	C 1s	288.0	3.4	C=O
(B) Photo-grafted PNP-film	C 1s	284.6	15.1	C-C aliphatic
	C 1s	285.6	68.1	C-O Ether
	C 1s	287.2	14.2	π to π* transition OR shifted C=O
	C 1s	291.9	2.5	Shake-up (π to π* transition)

This potentially universal photo-grafting approach was expected to covalently bind PNPs to phthalimide-functionalized surfaces and thereby alter the atomic composition at the surface. XPS of the samples before and after photo-grafting PNPs supports the occurrence of this photochemical reaction. Using UV exposure to graft PNPs demonstrates several changes by XPS, including a higher C/Si ratio and PNP-specific carbon components in the fitted high-resolution spectra.

3.3.2 Atomic Force Microscopy (AFM) Results

AFM analysis further supports the presence of photo-grafted PNPs on silicon substrates. AFM imaging can address the question: *How do the PNPs behave when spin-coated onto a surface from a stable, aqueous solution?* A previous model suggests that lateral capillary forces may influence particles to aggregate during the drying stage/spin-coating in order to find stability.[18] Spin-coating the PNPs onto the surface allows for dry deposition of the PNPs by evaporating the solvent. As a result, the glass transition temperature (T_g) is expected to increase and the polymer chains become frozen on the surface. Since the particles are polymeric, the PNPs may be more susceptible to surface rearrangement such that the higher energy functional groups may be buried in the bulk of the film.[19] However in our case, because the PNPs are vitrified at the core, the particles are expected to stay intact and keep the PS material within the PNP core and PEG material exposed to be in contact with the surface.

AFM allows us to probe nanoscale-deep into the structure of PNP-films and explore how capillary forces may or may not play a role in how the particles arrange themselves on a surface. AFM height images can be used to determine the root-mean-

square (rms) roughness of surfaces. The rms roughness describes the rms value of the surface height relative to the center place.[20]

Figure 3-5a shows an AFM image with 5.0 × 5.0 μm dimensions for a phthalimide SAM-functionalized silicon substrate that reveals a low rms value of 0.897 nm. However, as indicated by the AFM image of 10.0 × 10.0 μm dimensions, once the PNPs are photo-grafted onto the surface, the rms value increases to 3.52 nm (Figure 3-5b). The rms roughness is influenced by various factors which include the sharpness of the AFM tip, size of the nanoparticles, and packing density of the nanoparticle-film.

Rough qualitative analysis of the AFM image in Fig. 4b suggests that the NP-film does not have high surface coverage. The depth profile of this AFM image illustrates each featured particulate on the surface to be approximately 15 nm by 750 nm, height by width (Figure 3-5c). The dimensions of the featured particulates are larger than expected as each PNP in aqueous solution is estimated to be 100 nm in diameter.

A) B)

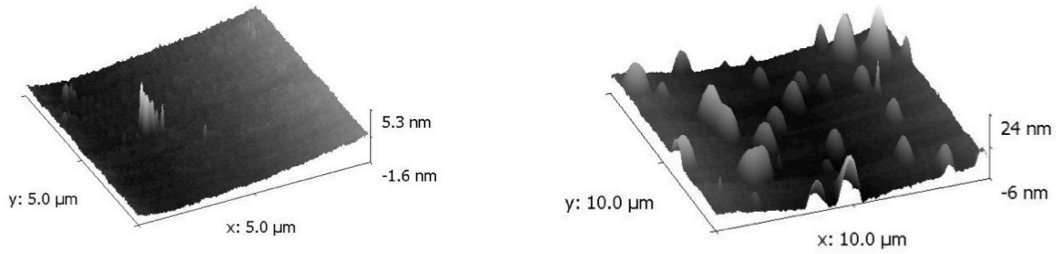

C)

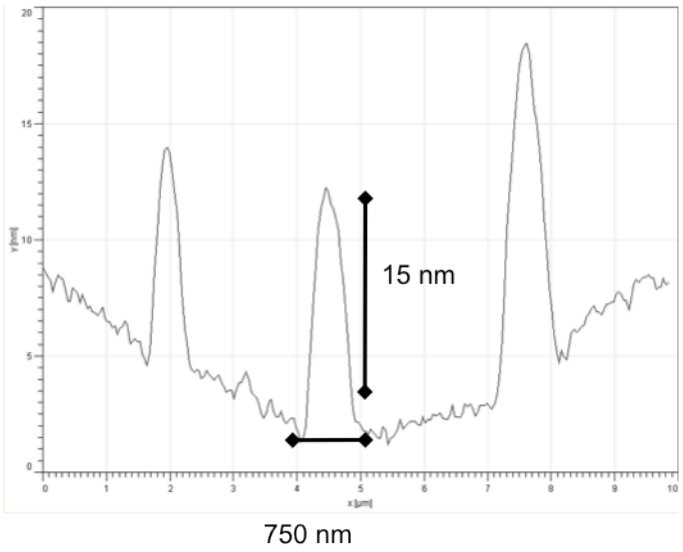

Figure 3-5. Atomic Force Microscopy (AFM) images of (A) phthalimide SAM on silicon wafer and (B) PNP-film on phthalimide-functionalized silicon wafer, and (C) the depth profile for line crossing of PNP-film in B.

The resulting outcome suggests two possibilities. The first possibility is that the PEG chains may have a strong affinity to the surface while the PS core may not be high enough in glass transition temperature T_g to be rigid, therefore upon drying the capillary forces flatten the particles onto the surface. Addressing the first possible cause is more difficult than the second because it involves altering the nature of PNPs themselves. The

second possibility for the large dimensioned features is that the PNPs may aggregate on the surface to find stability in the form of mini-islands. PNPs are initially stable and well dispersed in solution, but the final presence (or not) of aggregates is linked to the key balance between the inter-particle surface interactions and the capillary forces.

Thill et. al.[18] collected AFM images of four different scenarios – describing the effect of the capillary forces, in opposition to adhesion forces, on NP-film formation. There are three factors in favor of the lateral capillary forces: (1) large surface coverage of the NPs (i.e. short distance between the adsorbed particles), (2) the wettability and size of particles, and (3) the surface tension of the liquid film. It is difficult to predict and control the balance between adhesion and capillary forces and in general, it is not clear whether the capillary forces will affect the layer structure when drying onto a surface.

Comparing our PNP-film with a similar system presented by Thill et. al., we observe some similarities in the conditions of the NP-film preparation and in the AFM images of the fabricated films, seen in Figure 3-6. The AFM image on the right is indicative of a film where the lateral capillary forces seem to outweigh the adhesion forces. The adhesion forces do exist, but they are weak and as a result, some aggregation is observed.

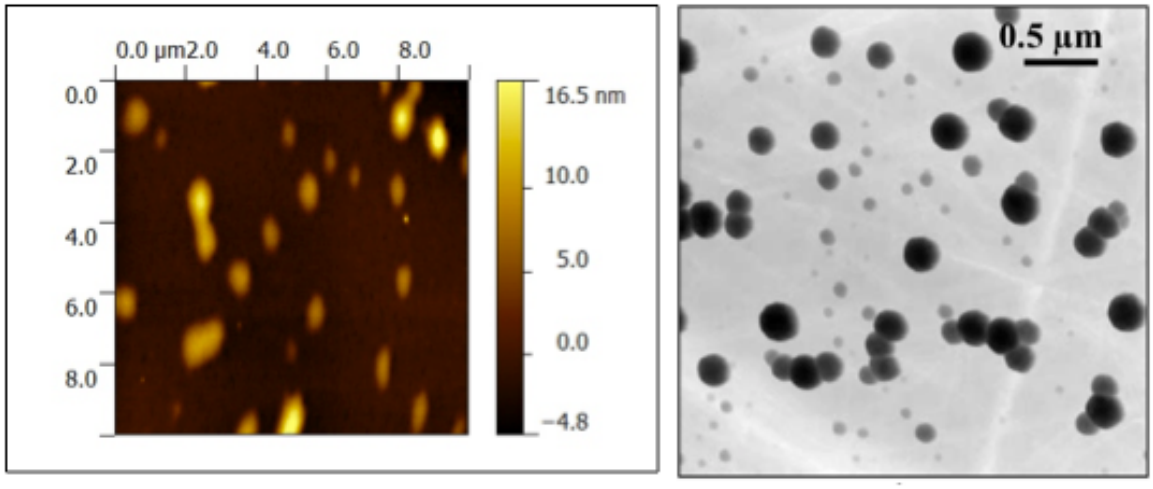

Figure 3-6. AFM images of photo-grafted PNP-film with 10.0 × 10.0 µm dimensions (left; experimental) and polydispersed latex particles adsorbed on Al2O3 surface presented in literature with 3.0 × 3.0 µm dimensions (right, literature[18]).

While it may not be possible to completely eliminate the aggregation effects, we may be able to control this balance and reduce the magnitude of aggregation by optimizing the synthesis and surface application of PNPs. One approach is to decrease the PNP solution concentration before spincoating them onto the surface. However, the purpose of this study is to demonstrate and prove a rapid and efficient method that covalently bonded nanoparticles onto a surface using light, different from current techniques available.

3.3.3 Confocal Fluorescence Microscopy (CFM) Results

Confocal Fluorescence Microscopy illustrates a unique feature of the photo-grafting approach – the ability to pattern nanoparticle-films, as illustrated in Figure 3-7. CFM was able to detect and image the presence of PNPs by using the dye-cores as visual indicators. Preliminary analysis detected a photo-bleaching complication that weakened the dye's fluorescence in the photo-grafting step of sample preparation.

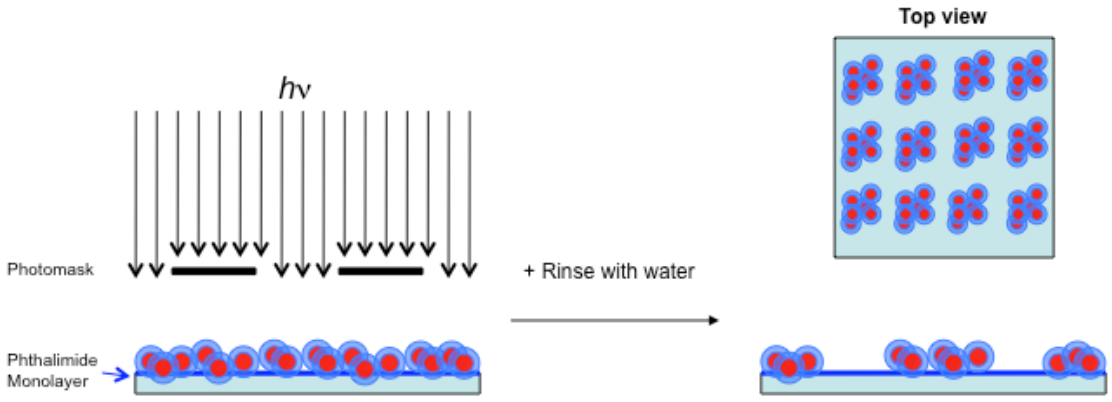

Figure 3-7. Schematic Illustration of photopatterning nanoparticles to a phthalimide-functionalized surface with use of photomask. (a) Only NPs that are exposed to hv covalently bond to the surface. (b) The expected pattern is due to unreacted NPs being washed away.

The image in Figure 3-8a is produced by a mask comprising a series of 50 micron squares. During the photo-attachment step in PNP-film fabrication, some photo bleaching of the fluorescent dye in the PNP cores is observed. The fluorescence intensity inside the square domains (light-exposed regions) was weaker than that of the surrounding gridlines that were protected from the light by the mask. The light-exposed square domains represent areas where PNPs were covalently attached to the surface. At this irradiation step before rinsing, we did not expect to detect a pattern of fluorescence, but the image in Figure 3-8a displays a pattern due to photo-bleaching. After rinsing the irradiated surface to remove unattached PNPs, we observe the expected fluorescence pattern, where fluorescent PNPs are present inside the bright square domains and absent along the dark borderlines. The confocal image, Figure 3-8b, shows the fluorescent 50-micron square domains that demonstrate successful surface attachment and patterning. Notice the decrease in overall fluorescence intensity from (a) to (b) and worsened S/N ratio as indicated by the plot profiles below each confocal image in Figure 3-8. Despite

the decreased image resolution, the expected fluorescent pattern is clearly seen, resulting from the PNP presence inside the square domains and no PNP presence in dark gridlines. When comparing these results to the dark controls, we do not observe this "photo-bleaching effect" because the irradiation step is eliminated. As a result, the dark controls of PNP-films (not exposed to light) exhibit a strongly fluorescent confocal image with no pattern to be seen.

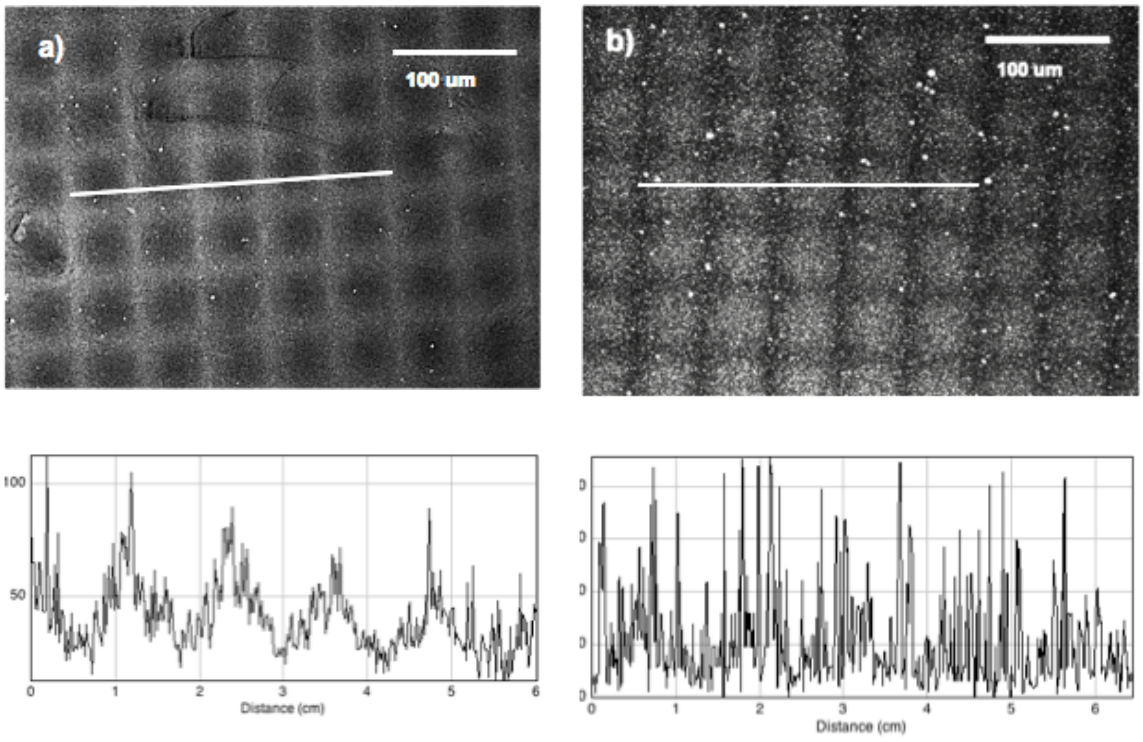

Figure 3-8. Confocal Fluorescence Microscopy image. CFM images of photopatterned NP-films on glass surface (a) before and (b) after rinsing away unreacted particles (Dye was excited at 488 nm). The contrast and brightness of CFM images were modified to distinguish pattern features. 20% alkyne terminated H-red PS/PEG particles were used. The pattern features were created using a TEM grid with 50-μm dimensions on each square. The bright, lighter regions represent the presence of fluorescent PNPs and the darker regions indicate no PNP presence. ImageJ software was used to produce the plot profiles below.

3.4 Summary and Outlook

Polymeric NPs were successfully photo-grafted and patterned onto hard substrates. XPS and AFM results indicate characteristic changes before and after PNPs are covalently bonded to the surface, while the CFM images demonstrate the patterning capacity of the universal photo-grafting method to fabricate NP-films. For future applications, the alkyne functionality of PNPs can be used to advance the design of biological interfaces by selectively "clicking" azide-functionalized biomolecules to the NP-films.

The unique feature of these PNPs is the alkyne-decorated outer shell. With the PNPs' alkyne functionality, the block copolymer nanoparticles hold promise in a number of fields including drug delivery.[21] The alkyne-functionality of PNP-films and its natural click chemistry capacity can advance the design of biologically active interfaces that require strong, specific attachment of biological ligands onto surfaces.[22]

3.5 Acknowledgements

We thank Professors Robert Prud'homme and James Link at Princeton University for the opportunity to collaborate on this research and Siyan Zhang, a graduate student in Prud'homme and Link research group, who synthesized the polymeric nanoparticles.

3.6 References

1. (a) Lu, Y.; Fan, H.; Stump, A.; Ward, T. L.; Rieker, T.; Brinker, C. J., Aerosol-assisted self-assembly of mesostructured spherical nanoparticles. *Nature* **1999,** *398*, 223; (b) Mirkin, C. A.; Letsinger, R. L.; Mucic, R. C.; Storhoff, J. J., A DNA-based method for rationally assembling nanoparticles into macroscopic materials. *Nature* **1996,** *382*, 607; (c) Majetich, S. A.; Jin, Y., Magnetization directions of individual nanoparticles. *Science* **1999,** *16*, 284; (d) Taton, T. A.; Mirkin, C. A.; Letsinger, R. L., Scanometric DNA Array Detection with Nanoparticle Probes. *Science* **2000,** *289*, 1757.

2. Wang, Y.; Zhong, W.; Jiang, N.; Yang, W., Directly Fabricating Monolayer Nanoparticles on a Polymer Surface by a UV-Induced MMA/DVB Microemulsion Graft Polymerization. *Macromol. Rapid Commun.* **2005,** *26*, 87-92.

3. (a) Blodgett, K. B., Films Built by Depositing Successive Monomolecular Layers on a Solid Surface. *J. Am. Chem. Soc.* **1935,** *57*, 1007-1022; (b) Rengifo, H. R.; Chen, L.; Grigoras, C.; Ju, J.; Koberstein, J. T., "Click-Functional" Block copolymers provide precise surface functionality via spincoating. *Langmuir* **2008,** *24*, 7450.

4. Shon, Y. S.; Choo, H., [60]Fullerene-linked gold nanoparticles: synthesis and layer-by-layer growth on a solid surface. *Chem. Commun.* **2002**, 2560-2561.

5. Manoudis, P. N.; Tsakalof, A.; Karapanagiotis, I.; Zuburtikudis, I.; Panayiotou, C., Fabrication of super-hydrophobic surfaces for enhanced stone protection. *Surface & Coatings Technology* **2009,** *203*, 1322-1328.

6. (a) Ma, Y.; Qian, L.; Huang, H.; Yang, X., Buildup of gold nanoparticle multilayer thin films based on the covalent-bonding interaction between boronic acids and polyols. *J. Colloid Interface Sci.* **2006,** *295*, 583-588; (b) An, Y.; Chen, M.; Xue, Q.;

Liu, W., Preparation and self-assembly of carboxylic acid-functionalized silica. *J. Colloid Interface Sci.* **2007,** *311*, 507-513; (c) Riboh, J. C.; Haes, A. J.; McFarland, A. D.; Yonzon, C. R.; Van Duyne, R. P., Real-Time immunoassay in Physiological Buffer Enabled by Improved Nanoparticle Adhesion. *J. Phys. Chem. B* **2003,** *107*, 1772-1780; (d) Fu, Y.; Xu, H.; Bai, S.; Qiu, D.; Sun, J.; Wang, Z.; Zhang, X., Fabrication of a Stable Polyelectrolyte/Au Nanoparticles Multilayer Film. *Macromol. Rapid Commun.* **2002,** *23*, 256-259.

7. (a) Terekhin, V. V. V., Formation of ordered nanoparticle assemblies by block copolymer lithography methods. *Russian chemical reviews* **2011,** *80* (5); (b) Beh, W. S.; Kim, I. T.; Qiu, D.; Xia, Y.; Whitesides, G. M., Formation of Patterned Microstructures of Conducting Polymers by Soft Lithography, and Applications in Microelectronic Device Fabrication. *Adv. mater.* **1999,** *11*, 1038.

8. Beh, W. S.; Kim, I. T.; Qiu, D.; Xia, Y.; Whitesides, G. M., *Adv. mater.* **1999,** *11*, 1038.

9. Carroll, G. T.; Wang, D.; Turro, N. T.; Koberstein, J. T., Photochemical Micropatterning of Carbohydrates on a Surface. *Langmuir* **2006,** *22*, 2899-2905.

10. (a) Akbulut, M.; Ginart, P.; Gindy, M.; Theriault, C.; Chin, K.; Soboyejo, W.; Prud'homme, R. K., Generic Method of Preparing Multifunctional Fluorescent Nanoparticles Using Flash NanoPrecipitation. *Adv. Funct. Mater.* **2009,** *19*, 1; (b) Zhang, S.; Adamson, D. H.; Prud'homme, R. K.; Link, A. J., Photocrosslinking the polystyrene core of block-copolymer nanoparticles. *Polym. Chem.* **2011,** *2*, 665; (c) Zhang, S. Y.; Prud'homme, R. K.; Link, A. J., Block Copolymer Nanoparticles as Nanobeads for the Polymerase Chain Reaction. *Nano Letters* **2011,** *11*, 1723; (d) Kumar, V.; Adamson, D.

H.; Prud'homme, R. K., Fluorescent Polymeric Nanoparticles: Aggregation and Phase Behavior of Pyrene and Amphotericin B Molecules in Nanoparticle Cores. *Small* **2010,** *6*, 2907.

11. Johnson, B. K.; Prud'homme, R. K., Flash NanoPrecipitation of Organic Actives and Block Copolymers using a Confined Impinging Jet Mixer. *Aust. J. Chem.* **2003,** *56*, 1021.

12. (a) Huisgen, R.; Szeimies, G.; Mobius, L., 1,3-Dipolare Cycloadditionen. 32. Kinetik Der Additionen Organischer Azide An cc-Mehrfachbindungen. *Chem. Ber./Recl.* **1967,** *100* (8), 2494-2507; (b) Kolb, H. C.; Finn, M. G.; Sharpless, K. B., Click Chemistry: Diverse chemical function from a few good reactions. *Angew. Chem. Int. Ed.* **2001,** *40* (11), 2004-2021.

13. Turro, N. T., *Principles of Molecular Photochemistry: An Introduction*. University Science Books: Sausalito, CA, 2009.

14. Hwang, L. Y.; Gotz, H.; Hawker, C. J.; Frank, C. W., Glyco-acrylate copolymers for bilayer tethering on benzophenone-modified substrates. *Colloids and Surfaces B: Biointerfaces* **2007,** *54*, 127-135.

15. Wagner, C. D.; Naumkin, A. V.; Kraut-Vass, A.; Allison, J.; Powell, C. J.; Rumble, J. R., *NIST X-ray Photoelectron Spectroscopy Database*. Measurement Services Division of the National Institute of Standards and Technology (NIST) Technology Services: Washington, DC, 2003.

16. (a) Spells, S. J., *Characterization of Solid Polymers*. Chapman & Hall: London, UK, 1994; (b) Girardeaux, C.; Pireaux, J.-J., Analysis of Polystyrene (PS) by XPS. *Surface Science Spectra* **1996,** *4*, 130-134.

17. Louette, P., Poly(ethylene oxide) (PEO) XPS Reference Core Level and Energy Loss Spectra. *Surface Science Spectra* **2005,** *12*, 59-63.

18. Thill, A.; Spalla, O., Aggregation due to capillary forces during drying of particle submonolayers. *Colloids and Surfaces A: Physicochem. Eng. Aspects* **2003,** *217*, 143-151.

19. Koberstein, J. T., Molecular Design of Functional Polymer Surfaces. *J. Polym. Sci. B.* **2004,** *42*, 2942-2956.

20. Smith, P. F.; Chun, I.; Liu, G.; Dimitrievich, D.; Rasburn, J.; Vancso, G. J., Studies of Optical Haze and Surface Morphology of Blown Polyethylene Films Using Atomic Force Microscopy. *Polym. Eng. Sci.* **1996,** *36* (16), 2129.

21. Gu, F. X.; Karnick, R.; Wang, A. Z.; Alexis, F.; Levy-Nissenbaum, E.; Hong, S.; Langer, R.; Farokhzad, O. C., Targeted Nanoparticles for Cancer Therapy. *NanoToday* **2007,** *2*, 14-21.

22. (a) Langer, R.; Tirrell, D. A., Designing materials for biology and medicine. *Nature* **2004,** *428*, 487-492; (b) Nandivada, H.; Chen, H.; Bondarenko, L.; Lahann, J., Reactive Polymer Coatings that "Click". *Angew. Chem. Int. Ed.* **2006,** *45*, 3360-3363.

4 Outreach: Oyster Restoration Project

4.1 Introduction

Recently, there has been great interest in using oysters as an environmental remediation tool in coastal ecosystems. Oysters have an advantage over other bivalve species to filter large quantities of heavy metals due to their habitat and feeding nature. Our research focuses on the eastern oyster species, *Crassostrea virginica,* that were re-introduced into the New York Harbor Estuary. We are interested in the quantitative analysis of the oysters' heavy metal intake by monitoring levels of metals such as Arsenic and Cadmium in their tissue and shells. The purpose of this research is to acquire baseline chemical data and evaluate the ecological health of the New York Harbor Estuary over a long period of time.

4.1.1 History of Oysters in New York Harbor and Project Background

In the 1800s, oysters were once prevalent in the New York Harbor for thousands of years, but have undergone a major decline from harsher conditions due to prolonged fishing pressure, habitat degradation and loss, and other stresses in the last one hundred years.[1] Oyster reefs make a significant contribution to the estuary water quality and health as they promote the presence of other filter feeders and fishes that could be as important as oysters for their filtration ability.

In August of 2009, the Hudson River Foundation brought together a team of oyster experts to proceed with the development of 6 experimental oyster reefs that were constructed in 2010. Besides the Foundation, other main participants in the Oyster Restoration Project include the NY/NJ Baykeeper, New York City Department of Parks

and Recreations Natural Resources Group, and the Urban Assembly New York Harbor School. The following section will introduce one of the 6 oyster sites in the estuary.

4.1.2 Recent Oyster Restoration efforts: Flupsy

Recent efforts have been made for oyster restoration in the harbor through an innovatively designed oyster nursery raft called a Floating Upweller System (flupsy), as shown in Figure 4-1. Flupsy has been a proven method to culture small shellfish seed through their delicate "nursery" stage, from coming out of a hatchery to being large enough to be sorted on a tray. Water flow and feed are increased to boost the growth of oyster seed in this system. Due to the force up-flow conditions, the seed grows at high densities much more quickly and uniformly, compared to the natural flow conditions. Therefore, the oysters are smaller in size than its peers that grow in better water quality conditions. A disclaimer for these young New York Harbor oysters is that they are not deemed edible by FDA standards due to their high levels of mercury and other toxic contaminants.

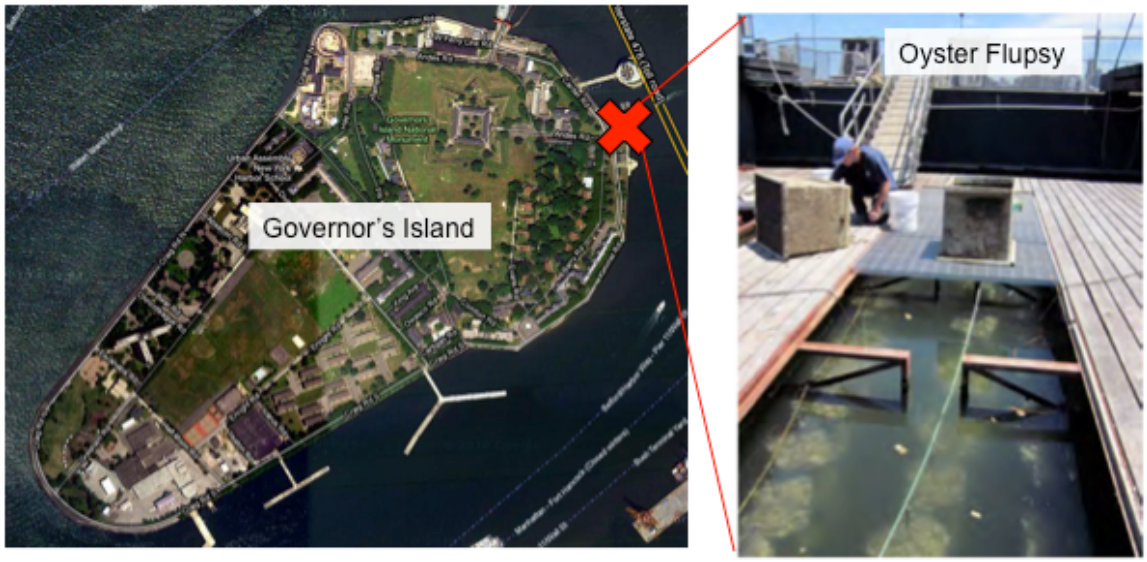

Figure 4-1. Oyster Flupsy at an Eco-Dock on Governor's Island. Satellite view of Governor's Island (left) provides the geographic location of the oyster flupsy (right).

4.2 Experimental Methods

Extensive research efforts have taken place that clearly demonstrate the special ability that oysters have to filter heavy metals from surrounding bodies of water.[2] We designed an experimental protocol similar to that used in an Australian study[3] to collect oysters and detect heavy metal concentrations from their body tissue and shells. For thorough analysis, three sample groups will be collected: 1) 3-year oysters from Harbor Flupsy, 2) Control I: 3-year old Fisher's oysters (same age as harbor oysters) and 3) Control II: Small size Fisher's island oysters (same size as harbor oysters).

Sample preparation includes finely grinding the shell and tissues and dissolving into the right solvent for analysis. High Resolution Inductively Coupled Mass Spectrometer (ICP-Mass Spec) will be used to focus on the analysis and monitoring of the following trace metals: aluminum (Al), arsenic (As), cadmium (Cd), Chromium (Cr), Copper (Cu), iron (Fe), mercury (Hg), manganese (Mn), lead (Pb), and Zinc (Zn). Preliminary results analyzing oyster tissue and shells with Brookhaven National Laboratory's National Synchrotron Light Source (NSLS) indicate the presence of calcium, zinc, copper, iron, nickel, and mercury, in decreasing order of concentration. However, more detailed studies are needed, in relation to oyster age, oyster size, timing of measurements, and temperature of waters.

4.3 Acknowledgements

Harbor School students and teachers play an integral role in the research efforts to monitor the changes in water quality and oyster metal intake. GK-12 LEEFS fellowship has given me the opportunity to work with the Harbor School on New York City Oyster

restoration project and integrating some research in the chemistry curriculum. We thank Peter Malinoswki and Roy Arezzo for providing assistance with the oyster project.

4.4 References

1. (a) Kurlansky, M., *The Big Oyster: History on the Half Shell*. Ballantine Books: New York, 2006; (b) Luckenbach, M. W.; Coen, L. D.; Ross, P. G. J.; Stephen, J. A., Oyster reef habitat restoration: relationships between oyster abundance and community development on two studies in Virginia and South Carolina. *J. Coast. Res.* **2005,** *40*, 64-78.

2. (a) Abbe, G. R.; Riedel, G. F.; Sanders, J. G., Factors that influence the accumulation of copper and cadmium by transplanted eastern oysters (Crassostrea Virginica) in the Patuxent River, Maryland. *Marine Environmental Research* **2000,** *49*, 377-396; (b) Johnson, W. E.; Kimbrough, K. L.; Lauenstein, G. G.; Christensen, J., Chemical Contamination assessment of Gulf of Mexico oysters in response to hurricanes Katrina and Rita. *Environ. Monit. Assess.* **2009,** *150*, 211-225; (c) Frazier, J. M., The Dynamics of Metals in the America Oyster, Crassostrea Virginica. II. Environmental Effects. *Chesapeake Science* **1976,** *17*, 188-197.

3. Gifford, S.; Dunstan, H.; O' Connor, W.; Macfarlane, G. R., Quantification of in situ nutrient and heavy metal remediation by a small pearl oyster (Pinctada imbricata) farm at Port Stephens, Australia. *Marine Pollution Bulletin* **2005,** *50*, 417-422.